Int J Earth Sci (Geol Rundsch) (2017) 106:2067–2089
DOI 10.1007/s00531-016-1414-0

ORIGINAL PAPER

Geochemistry of mylonitic gneisses from the Cycladic Basement Unit (Paros and Serifos, Aegean Sea): implications for protoliths of the high-grade gneisses

Annette McGrath[1] · Christina Stouraiti[2] · Brian Windley[1]

Received: 5 January 2016 / Accepted: 14 October 2016 / Published online: 28 October 2016

Abstract The nature of the protolith(s) of high-grade gneisses from the Aegean Cycladic Basement Unit of the islands of Paros and Serifos is investigated using whole-rock geochemistry and Sr–Nd–O isotopes, in order to better understand their origin and to compare with possible equivalents from the southern Aegean region. On Paros, the basement unit consists of heterogeneous, mylonitized upper amphibolite-grade paragneisses and associated migmatitic rocks, whereas on Serifos, it consists of a mylonitized felsic gneiss, intercalated with layers and lenses of S-type leucogranites and minor mafic metavolcanics. New Nd, Sr and O isotope data suggest a predominantly crustal-derived source in the gneiss protolith from both islands: high initial $^{87}Sr/^{86}Sr$ ratios ($\geq$7052 to 0.711, calculated at 300 Ma), negative initial ε_{Nd} (-2.8 to -7.7) values for bulk-rock gneiss samples, and high $\delta^{18}O$ values of quartz separates ($+10$ to $+12.7$ ‰). Major and trace-element variations corroborate that chemical differentiation within the NW Paros gneiss subunit results from progressive migmatitization. Peraluminous gneisses from eastern Paros share clear similarities with metapelitic gneisses from the Naxos gneiss dome, in terms of their trace-element patterns, ε_{Nd} (300) and O isotope characteristics. The mineral assemblage, the fine grain size (due to intense mylonitization), and the metaluminous affinity of the South Serifos grey quartzofeldpathic gneiss do not allow for an unambiguous interpretation for these undated rocks; however, a combination of geochemical parameters and tectonic discrimination diagrams indicates an immature siliciclastic (greywacke) protolith from a continental island arc setting. Sr–Nd isotopic systematics indicates an increasing lower crustal component in gneisses from NW Paros, which is closer to the migmatitic core of the Paros dome. The overall isotopic trend of the gneissic Cycladic Basement Unit on Paros is spatially correlated with that of the Naxos gneiss dome.

Keywords Aegean · Ortho-paragneisses · Sr–Nd–O isotopes · Paros · Serifos

Introduction

The Attic-Cycladic Crystalline Complex (ACC; Fig. 1) of the Hellenides in the southern Aegean comprises an extensive metamorphic belt, lying to the north of the present Hellenic subduction zone. The structural evolution of the Hellenide Orogenic Belt (Fig. 1) in the Eastern Mediterranean region is related to an Alpine-type collision between Gondwana-derived fragments and the Eurasian plate (e.g. Altherr et al. 1982; Keay and Lister 2002). The Cycladic archipelago is a key area for understanding the structural evolution of the broader Aegean region. In various plate

Electronic supplementary material The online version of this article (doi:10.1007/s00531-016-1414-0) contains supplementary material, which is available to authorized users.

✉ Christina Stouraiti
chstouraiti@geol.uoa.gr

Annette McGrath
annettemcgrath@aol.com

Brian Windley
brian.windley@btinternet.com

[1] Department of Geology, University of Leicester, Leicester LE1 7RH, UK

[2] Division of Geochemistry and Economic Geology, Department of Geology and Geoenvironment, National and Kapodistrian University of Athens, Panepistimioupolis, 15784 Zografou, Athens, Greece

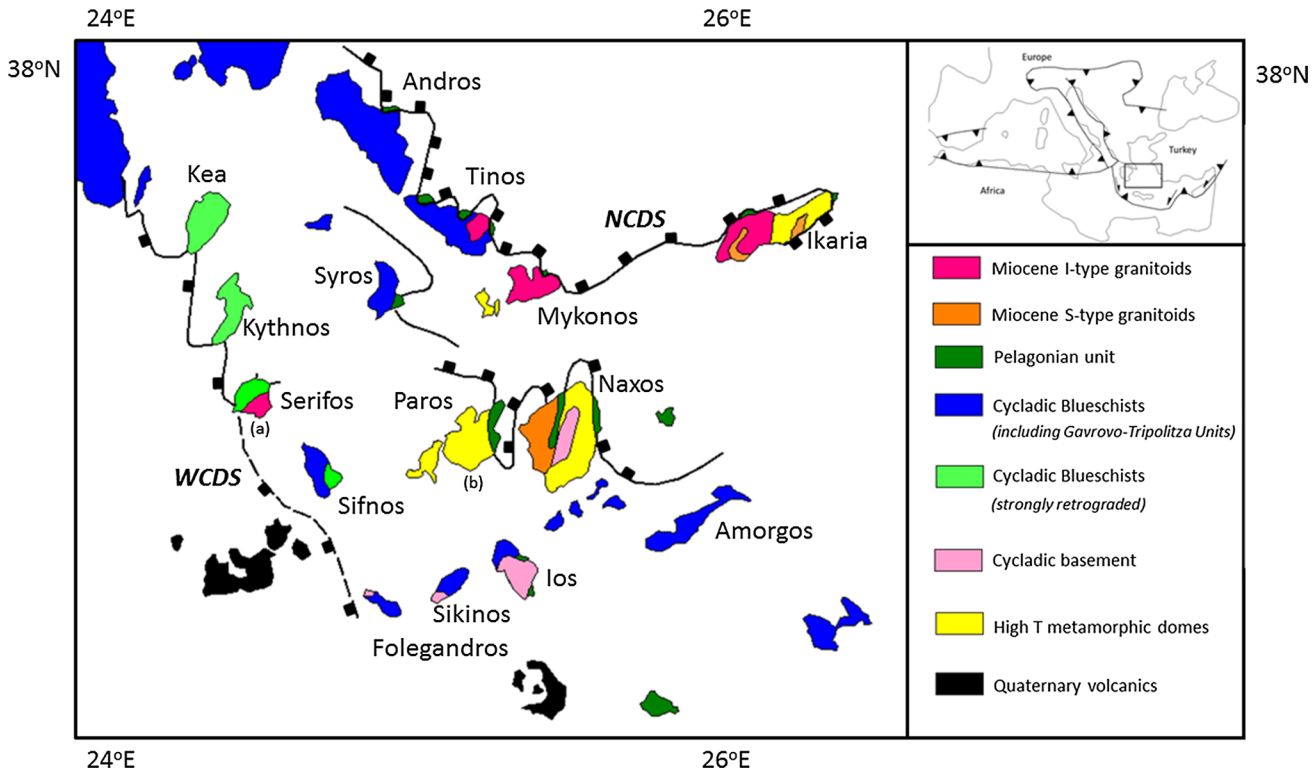

Fig. 1 Simplified tectonic map of the Cyclades archipelago showing the Attic-Cycladic Crystalline Complex and the main metamorphic core complexes. Distribution of the Cycladic Blueschist Unit (CBU), the Cycladic Basement rocks and the Pelagonian unit within the ACC is also shown (after Jolivet and Brun 2010; Jolivet et al. 2015, and references therein). *NCDS* North Cycladic Detachment System, *WCDS* West Cycladic Detachment System. *Insert*: map showing Miocene to recent thrust fronts in Mediterranean region and location of the main map. The (*a*) and (*b*) notations correspond to the locations of the study areas Serifos and Paros islands, respectively (see Fig. 2a, b)

tectonic models, it is generally agreed that rifting and drifting of Gondwanan microcontinental fragments were initiated during Late Carboniferous–Permian times and continued into early to mid-Triassic times, which eventually led to the opening of Neotethyan ocean basin(s) (Pe-Piper 1998 and references therein; Chatzaras et al. 2013; Fu et al. 2015). In most studies, the ACC is correlated along strike with the Pelagonian Unit of continental Greece and the metamorphic core complex of the Menderes Massif in western Turkey (Fig. 1; Papanikolaou and Demirtasli 1987).

In spite of many extensive studies of the Hellenides, there are unresolved questions concerning the litho- and/or tectono-stratigraphic relationships across the entire ACC. The structurally lower tectonic unit (=Cycladic Blueschist Unit, CBU) of the ACC is built up mainly by a metamorphosed volcano-sedimentary succession of Permo-Mesozoic age (e.g. Okrusch and Bröcker 1990; Löwen et al. 2015; Hinsken et al. 2015; Bröcker et al. 2016) that forms the cover sequence of a pre-Alpidic crystalline basement (Henjes-Kunst and Kreuzer 1982; Andriessen et al. 1987). Hercynian basement rocks have a coherent surface exposure in the southern Cyclades (Ios, Naxos, Sikinos: Henjes-Kunst and Kreuzer 1982; Van der Maar and Jansen 1983; Andriessen et al. 1987; Franz et al. 1993), but in the northern Cyclades, only remnants of them are preserved within the Cycladic Blueschist Unit (Syros: Tomaschek et al. 2008). Previous geochronological studies established the general geologic and metamorphic time frame of the Cycladic region (e.g. Dürr et al. 1978; Okrusch and Bröcker 1990; Jolivet and Brun 2010 and references therein), but there is still incomplete knowledge especially about: (a) the depositional ages of siliciclastic metasediments which make up large parts of the CBU (Löwen et al. 2015 and references therein), and also (b) the nature of the protoliths of the Cycladic basement gneisses.

U–Pb and Pb–Pb zircon geochronological studies of orthogneisses from the southern Aegean and the surrounding areas document several tectonomagmatic events in the Hellenides in late Carboniferous to Triassic times, which help to constrain the age of the basement units (Supplementary Table) into which they are intruded, and provides potential ages for their protoliths (e.g. Engel and Reischmann 1998; Vavassis et al. 2000; Xypolias et al. 2006;

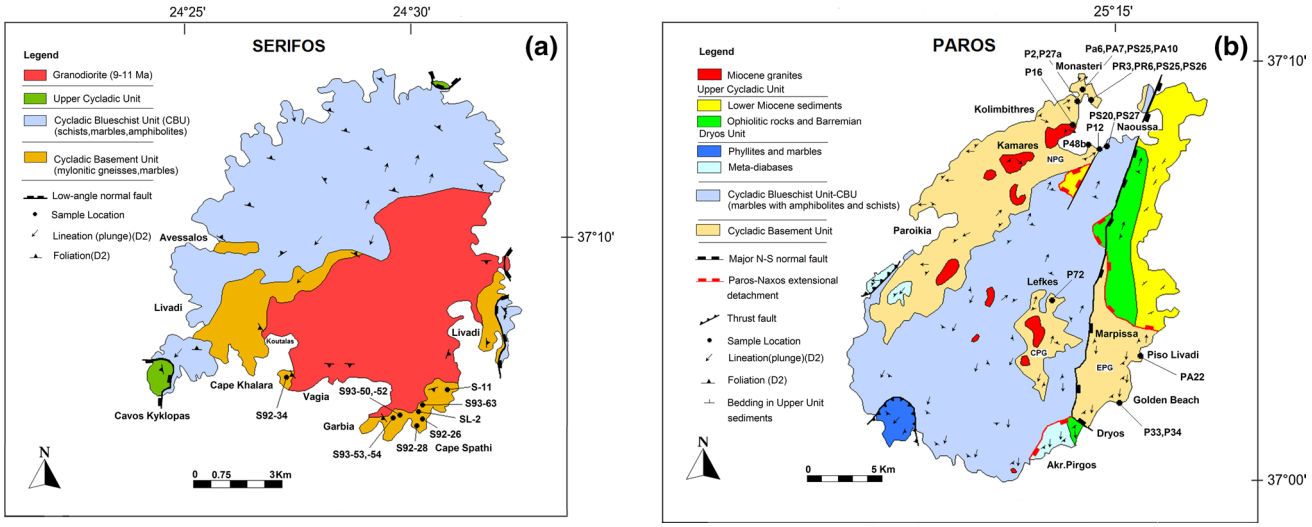

Fig. 2 **a** Simplified geological map of Serifos island with sample locations, as *black dots* (after Petrakakis et al. 2010; Grasemann et al. 2011). **b** Simplified geological map of Paros island with sample locations, as *black dots* (after Gautier et al. 1993; McGrath 1999; Bargnesi et al. 2013). *NPG* NW Paros gneiss, *EPG* East Paros Gneiss, *CPG* Central Paros Gneiss

Anders et al. 2007; Bröcker and Pidgeon 2007; Tomaschek et al. 2008). These studies established a late Carboniferous (330–295 Ma) magmatic age group for metagranitoids within the pre-Alpine basement units in Sikinos, Ios, Naxos, Paros, and central-northern Evia (Keay and Lister 2002; Engel and Reischmann 1998; Reischmann 1998; Vavassis et al. 2000; Photiades and Keay 2003).

SHRIMP U–Pb zircon and Pb–Pb zircon evaporation dating of acidic gneisses intercalated within melange units of the CBU on Andros, Sifnos, Ios, Naxos Islands, and Syros have mainly yielded Early–Middle Triassic (ca. 250–230 Ma) ages (Bröcker and Keasling 2006; Bröcker and Pidgeon 2007; Fu et al. 2015) and Late Triassic ages for the southern Evia metagranitoids (ID-TIMS U–Pb on single zircons: Chatzaras et al. 2013). Moreover, detrital zircons from the siliciclastic metasediment sequences from the Lower Unit (CBU) of different Cycladic islands indicate a supply from dominantly Triassic (and Late Paleozoic) source rocks and minor Jurassic to Cretaceous detritus (Syros: Löwen et al. 2015; Tinos: Hinsken et al. 2015; Ios, Andros, Syros, Sifnos: Fu et al. 2015). Based on the new age data, Bröcker et al. (2016) underlined the importance of the nearby Triassic igneous sources which corroborated a Late Jurassic-Early Cretaceous sediment accumulation for the broader northern Cycladic domain. Several tectonic models have been proposed concerning Triassic and subsequent magmatism (overview in Robertson 2012 and Chatzaras et al. 2013), but as yet no generally accepted interpretation has been established (Fu et al. 2015).

Here, we address the origin of the basement gneisses from Paros and Serifos. In south and south-western Serifos (Fig. 2a), the exposure of the Cycladic Basement Unit consists mainly of mylonitic gneisses (Fig. 2a; Grasemann and Petrakakis 2007; Iglseder et al. 2009). Previous studies could not deduce a single age for the protolith of these gneisses. Ages range from Triassic to Carboniferous attributed to the inherited and detrital nature of their analysed zircons (Schneider et al. 2011), unlike the typical Hercynian magmatic ages recorded in the basement orthogneisses in the southern Cycladic islands (e.g. Keay and Lister 2002). We suggest that the Serifos basement gneisses is a complex unit, and part of it may correspond to metamorphosed siliciclastic protoliths which are common in the Cycladic Blueschist Unit (CBU) (Hinsken et al. 2015).

With regard to Paros (Figs. 1, 2b), Engel and Reischmann (1998) and Reischmann (1998) postulated an igneous protolith for gneisses of the Cycladic Basement Unit, based on a study of euhedral, magmatic zircons, that indicated an intrusion age of circa 317 ± 2 Ma (Pb–Pb) for the presumed granitic precursor to the gneiss. However, we suggest that this interpretation is questionable as this age is based on only a few data points (see Supplementary Table). Moreover, the complex zircon populations of other samples from Paros suggest a detrital origin (Keay and Lister 2002), which reflects the complex history of this unit.

The aim of this study is to investigate the geochemical and isotopic characteristics of the mylonitic para- and ortho-gneisses from the Cycladic Basement Unit of Serifos and Paros. We present new major- and trace-element whole-rock analyses and O, Sr, and Nd isotope data combined with field relations and structural observations, in order to characterize their origin and source-rock lithologies. Comparisons are also made with other gneissic units

(both ortho- and paragneisses) of known composition and protolith from other Cycladic Basement Units and Triassic felsic rocks from the Lower Unit of the Cycladic Blueschists Unit (e.g. Naxos—Pe-Piper et al. 1997; Pe-Piper 2000; felsic gneisses from Syros—Tomaschek et al. 2008; metagranitoids from S Evia—Chatzaras et al. 2013) as well as clastic sediment sequences (greywackes from Chios—Meinhold et al. 2007) in an attempt to make regional correlations.

Regional geological setting

The Attic-Cycladic Crystalline Complex (ACC) (Fig. 1) consists of a tectonic stack of major units/nappes that were emplaced during the Alpine M1/D1 compressional metamorphic event (Altherr et al. 1982; Jolivet et al. 2003; Van Hinsbergen et al. 2005; Jolivet and Brun 2010) in post-Cretaceous times. The different tectonic slices were subsequently juxtaposed during Miocene extension (the M2a/D2 tectono-thermal event), along low-angle normal-sense detachment faults associated with metamorphic core complexes (Lister et al. 1984). The current configuration of tectonic units in the central Aegean is therefore the result of extensional reorganization of the early Alpine nappe stack (Bargnesi et al. 2013).

From the lowermost to the upper structural levels, the Cycladic units (Dürr et al. 1978; Okrusch and Bröcker 1990) consist of:

1. The Cycladic Basement Unit, which is composed of Hercynian ortho- and para-gneisses, schists, and amphibolites (Altherr et al. 1982; Henjes-Kunst and Kreuzer 1982; Andriessen et al. 1987; Bolhar et al. 2010). This basement is exposed on several islands as metamorphic core complexes (e.g. Lister et al. 1984; Gautier et al. 1993; Gautier and Brun 1994). On Paros (Fig. 2b), Pb/Pb dating of basement gneiss units yielded ages of 302(±2) to 325(±4) Ma (Supplementary Table), which has been interpreted to indicate that magmatism was broadly contemporaneous with Variscan metamorphism (Engel and Reischmann 1998; Bargnesi et al. 2013).
2. The overlying Cycladic Blueschist Unit (CBU) consisting of a possible post-Carboniferous shelf sequence of marbles, metapelites, and metavolcanic rocks (Dürr et al. 1978). The CBU is characterized by a change in the nature of the protolith between the northern and southern area (Papanikolaou 1987, 1989). The southern CBU is exposed in the central-southern parts of the Cyclades (Paros–Naxos) and consists of a sequence of continental origin. The northern CBU (Syros, Andros and Tinos) is derived from a pelagic volcano-sedimentary sequence which contains no exposed basement (Katzir et al. 2007).
3. The structurally higher unit (=Upper Cycladic Unit) locally overlies the CBU. It is a poorly preserved heterogeneous sequence. It consists of dismemberd ophiolites, greenschist- to amphibolite-facies rocks with Cretaceous to Tertiary metamorphic ages, and felsic gneisses, intercalated with Permian to Mesozoic marbles, covered by un-metamorphosed carbonates (e.g. Dürr et al. 1978; Bröcker and Franz 1998).

The Alpine metamorphic history of the Cycladic units includes two successive tectono-metamorphic events: a high-pressure (HP) M1 (D1) event at circa 45 Ma and a regional Barrovian-type M2a (D2) metamorphism between 23 and 16 Ma (Altherr et al. 1982; Andriessen et al. 1987; Wijbrans and McDougall 1988). In the central Cyclades, basement gneisses were locally migmatized (the M2b event), at upper amphibolite facies (670 ± 50 °C, 5–7 kbar; Buick and Holland 1989), as recorded in the Naxos and Paros domes (Wijbrans and McDougall 1988; Buick 1991; Gautier et al. 1993; Keay et al. 2001). On Naxos the timing of peak M2b metamorphism and migmatitization is well constrained to between 19 and 14 Ma, based on U–Pb dating of metamorphic zircon growth from amphibolite-facies rocks (Keay et al. 2001; Martin et al. 2006). On Naxos (Fig. 2c), a classic example of a systematically studied gneiss dome, the core consists of migmatized Mesozoic-age (Alpine) metasediments or S-type granitoids, interlayered with thin slivers of Hercynian orthogneiss (Buick 1991; Keay et al. 2001). This study focuses on both Paros and Serifos and provides new data from the less-studied Paros gneissic Cycladic Basement Unit.

Paros geology

The island of Paros (Fig. 2b) was traditionally recognized by Papanikolaou (1980) to consist of three nappes, the Marathi (Lower), Dryos (Intermediate) and Marmara (Upper) Nappes. Detailed structural mapping of Paros (Gautier et al. 1993; McGrath 1999; Bargnesi et al. 2013) subsequently distinguished a succession of major low-angle extensional detachment faults, separating highly metamorphosed and mylonitized crustal rocks in the footwall from weakly- to un-metamorphosed sediments and ophiolitic rocks in the hangingwall (the Upper Cycladic Unit of Fig. 2b), forming a metamorphic core complex. D2 mylonitic foliation and lineation indicate that the whole island has a dome-like architecture (the main Paros gneiss dome, Fig. 2b).

The Cycladic Basement rocks of Paros (the Cycladic Basement Unit of Fig. 2b, formerly known as the lowermost part of the "Marathi Nappe" after Papanikolaou 1980)

are a series of highly deformed Carboniferous ortho- and para-gneisses (Engel and Reischmann 1998), metamorphosed to upper greenschist to upper amphibolite facies. The gneissic units can be found in three major sections on Paros (Fig. 2b): (1) on the western side of the island, from Monasteri-Naoussa Bay in the north-west to southern Paroikia in the west (the NW Paros gneiss; NPG on Fig. 2b), (2) the centre of the island, south of Lefkes (the Central Paros gneiss; CPG on Fig. 2b), and (3) on the east to south-eastern section of the island, from Piso Livadi and Marpissa to Golden Beach and Drios in the south (the East Paros gneiss; EPG on Fig. 2b). In some horizons, the gneisses are highly migmatized, hosting a series of S-type pegmatitic and aplitic sills and dykes, garnetiferous leucogranites, and larger-scale biotite-rich granites (the "Miocene granites" of Fig. 2b). At the contact with the detachment faults, the gneisses are variously intercalated with millimetre- to decimetre-scale mylonitized marble horizons, which increase in abundance towards the detachment fault contact and the overlying Upper Cycladic Unit.

This gneissic Cycladic Basement Unit is overlain by a series of tectonically intercalated marbles, amphibolites, and mica-schists, formerly known as the uppermost Marathi Nappe (Papanikolaou 1980). The latter unit (Marathi Nappe) is now considered to correlate with the Cycladic Blueschist Unit (CBU, in Fig. 2b; Bargnesi et al. 2013). However, the subsequent M2a greenschist to lower amphibolite facies Barrovian metamorphism over-printed and mostly obliterated the HP "blueschist" signature on Paros (e.g. Gautier et al. 1993; McGrath 1999), so the unit is not a blueschist unit, sensu stricto.

The Dryos Unit (Fig. 2b) is a very low-grade, structurally intermediate level nappe (overlying the CBU) possibly of Permian age (the Dryos Nappe of Papanikolaou 1980). The lithological sequence consists of marbles, phyllites, and metabasic rocks (the "meta-diabases" of Papanikolaou 1980).

The Upper Cycladic Unit (formerly the uppermost "Marmara Nappe" of Papanikolaou 1977, 1980; Fig. 2b) consists of an un-metamorphosed to very low-grade sequence of Cretaceous-age (Barremian) limestones, Lower Miocene basinal siliciclastic sediments, and serpentinized ophiolitic fragments. The Upper Cycladic Unit is exposed along the eastern coastline of the island, extending from Piso Livadi and Marpissa in the south, to the northern tip of the island (NNE of Naoussa), and also in a series of small sections south of Drios and close to and south-west of the village of Naoussa (Fig. 2b).

Serifos geology

The island of Serifos (Fig. 2a) has a dome-like architecture, dominated by a late-Miocene granitoid intrusion which intruded at a shallow crustal level (Brichau et al. 2010; Stouraiti et al. 2010). The pluton intruded syn-kinematically into an extensional shear zone between 11.6 and 9.5 Ma (Iglseder et al. 2009; Rabillard et al. 2015). Two tectonic units are recognized on Serifos (Grasemann and Petrakakis 2007; Grasemann et al. 2011; Iglseder et al. 2009): (a) the Cycladic Basement Unit (Fig. 2a) which is structurally the lowermost and consists of a thick (>200 m; Grasemann et al. 2011) sequence of mylonitic orthogneisses, schists, and siliceous rocks with gneissic fabric; this unit is over- and underlain by mylonitic marbles with gneiss intercalations; (b) the overlying Cycladic Blueschist Unit (Fig. 2a), consisting of amphibolites intercalated with thin layers of gneiss, metabasites, felsic greenschists, carbonate schists, and marbles. The Cycladic Blueschist Unit sequences from Serifos preserve relic evidence of the M1 (HP) event (e.g. phengite and relict glaucophane), that was subsequently overprinted by the regional M2 greenschist to lower amphibolite facies metamorphism (Iglseder et al. 2009; Tschegg and Grasemann 2009).

Previous studies considered the lower structural unit in Serifos to represent a pre-Alpine basement of orthogneiss or earlier S-type granitoid that was mylonitized during SSW-directed exhumation at mid-crustal levels (Grasemann and Petrakakis 2007; Iglseder et al. 2009; Schneider et al. 2011). However, the nature of the protolith(s) of these gneisses remains unclear and is the subject of this study.

Lithology and petrology

The NW Paros Cycladic Basement gneiss

The high-grade NW Paros gneisses (NPG) and associated migmatitic rocks crop out in a broad NE-SW trending swathe from north-west Paros to southern Paroikia (Fig. 2b). Both the gneiss and migmatites show varying intensities of mylonitization and have strong L-S fabrics. The upper amphibolite facies gneiss has a mineralogy of mainly biotite, muscovite, quartz, plagioclase, cordierite, and alkali feldspar ± sillimanite, that also define the mylonitic foliation and mineral stretching lineation. Garnets are extremely rare, and when present are strongly retrogressed to biotite and chlorite. The gneisses in NW Paros are heterogeneous on a meso- to macro-scale, and comprises layers of coarser-grained light-grey quartz- and feldspar-rich gneiss intercalated with horizons of darker biotite-rich gneiss, that are parallel to the mylonitic foliation. Intense D2/M2 mylonitization produced homogenization of the precursor, but rare pockets and lenses of less-metamorphosed material within the gneiss indicate a potential sedimentary origin. These lenses contain rounded quartz grains, as opposed to interlocking grain boundaries, suggesting that they are

remnants of clastic fragments. Decimetre-scale alternations of darker (biotite-rich) and lighter (quartz- and muscovite-rich) horizons in the gneiss, parallel to the mylonitic foliation, may therefore reflect the original metasedimentary bedding. We therefore suggest that the protolith of the NW Paros gneiss consisted of a mixed pelite/psammite clastic sediment derived from a bedded greywacke–shale sequence, rather than a deformed biotite granite as suggested by other authors (Andriessen et al. 1979; Engel and Reischmann 1998; Schneider et al. 2011). Intense tectonic homogenization and intermixing of the sediments occurred during the subsequent D2/M2 mylonitization event, leaving evidence of original sedimentary compositional variations only on a larger, decimetre scale. However, examination of the bulk-rock and isotope geochemistry will help to discriminate between alternatives (sections "Bulk rock geochemistry" to "O isotopes").

The east Paros Cycladic Basement gneiss

The East Paros gneisses crop out in a broad coastal expanse from Golden Beach in the south, to Piso Livadi and Marpissa in the north (EPG, Fig. 2b). North of Piso Livadi, the gneisses are juxtaposed against weakly- to un-metamorphosed sediments of the Upper Cycladic Unit (the former "Marmara Unit", after Papanikolaou 1980) below a shallowly north-dipping extensional detachment surface (Fig. 2b). The gneisses continue inland to the west, where they are truncated by marbles and amphibolites of the Cycladic Blueschist Unit along a major N-S fault (Fig. 2b). Papanikolaou (1980) considered that the East Paros gneiss correlate with the NW Paros gneisses, which superficially do appear to be very similar as both units display L–S tectonite fabric. However, closer examination suggests significant differences. Southerly sections of the East Paros gneiss, around Golden Beach (Fig. 2b), are less deformed and metamorphosed than the average NW Paros gneiss, and resemble a mica schist sensu stricto rather than gneiss. The intensity of deformation and gneissose metamorphic texture in the East Paros gneiss unit also increases significantly from south to north, towards the footwall of the detachment fault north of Piso Livadi, where the gneisses are characterized by intense deformation, as indicated by ultramylonitic and L-tectonite fabrics. However, a small locality south of Golden Beach, farthest away from the detachment fault, highlights the lithological and structural variety within the East Paros gneiss/schist unit, and occupies the least deformed area along the section. Here, the East Paros gneiss unit includes lower-grade mica schist (Table 1, sample P36), which grades northwards into "gneiss" with a mineralogy of biotite and muscovite, plagioclase, orthoclase, quartz and opaque minerals, and is thus similar in composition to the NW Paros gneiss, albeit less deformed and metamorphosed. In localized horizons, the East Paros gneiss contain enclaves of lower-grade mica schist that retain their pre-metamorphic fabrics, and even preserve pockets of its sedimentary protolith (Sample P36, Table 1). Pronounced decimetre- to metre-thick layers of coarse quartz-rich schist (interpreted to be former psammitic layers) alternate with darker, more micaceous horizons (interpreted to be former pelitic layers), representing original variegated sand- and mud-rich greywacke sediment layers.

The southern Serifos Cycladic Basement gneisses

On the basis of field and textural evidence, two types of quartzo-feldpathic gneisses occur in the Cycladic Basement Unit of South Serifos: a) medium to fine-grained, grey quartzo-feldspathic gneisses, and schists (the South Serifos grey gneiss) that contain b) pale leucogneiss/leucogranites (the South Serifos leucogneiss), which occur in lenses or dykes of variable thickness (from a few cm up to 1 m thick), conformable to the general foliation. Extreme mylonitization has been recorded from the higher structural levels of this unit, especially within quartzitic horizons. Previous studies described the mylonitic gneiss from the structurally Lower Unit of Serifos as an orthogneiss (Iglseder et al. 2009), which was thought to represents an earlier stage of magmatism, whereby the mylonite is an S-type granite that syn-kinematically intruded into a mid-crustal shear. A later study by Schneider et al. (2011) showed that this mylonite lacks magmatic zircons but contains xenocrystic Triassic–Carboniferous zircons that have witnessed Eocene recrystallization, as evidenced by a relict HP metamorphic assemblage (Qtz + Fsp ± Chl ± Phg ± Stp).

The South Serifos grey gneisses are the most common type of gneiss, consisting of quartz + plagioclase + K-feldspar + biotite + muscovite + sphene and abundant Fe–Ti oxides; minor chlorite has replaced biotite. Only in one location in south-west part of Serifos (Cape Khalara roof pendant, Fig. 2a) is it possible to recognize the preserved primary sedimentary bedding on a centimetre-scale. Compositional layering is formed by dark biotite-rich and light plagioclase-rich layers (defined as individual beds) separated by millimetre-thick quartz-rich beds. Within this unit, there were recognized gneisses with texture and composition similar to acid volcanic rocks, i.e. meta-tuff. The heterogeneous lithological assemblage of quartzitic-, quartzo-feldspathic-, biotite-rich bands, marbles, and metavolcanics (metatuffs), alternating on a mesoscopic to macroscopic scale, indicates a rather complex clastic sedimentary sequence as opposed to a block of crystalline basement. However, the small grain size (due to mylonitization) and mineral assemblage of the South Serifos grey gneiss do not allow for an unequivocal assignment of a unique rock type without ambiguity (either a meta-granitoid or a siliciclastic sediment).

Table 1 Representative whole-rock analyses (XRF) of major elements (wt%) and trace elements (ppm) of (a) Serifos and (b) Paros mylonitic gneisses

Sample no.	S-11	S92-28	S93-50	S93-53	S92-26	S93-54	S93-63	S Leu-2	S92-34	S93-52
Rock unit	GQFG	GQFG	GQFG	GQFG	GQFG	LG	LG	LGr	LG (Quartzitic)	LGr
(*a*) *South Serifos*										
SiO_2	70.7	69.2	71.1	62.6	60.2	79.4	77.9	78.4	78.3	78.8
TiO_2	0.6	0.4	0.6	0.6	0.767	0.1	0.019	0.08	0.14	0.11
Al_2O_3	13.7	15.8	13.6	15.6	16.8	11.7	13.2	12.4	10.4	11.9
Fe_2O_3	4.3	3.4	4.3	4.2	8.5	1.3	0.8	1.2	1.8	1.4
MnO	0.09	0.1	0.1	0.1	0.12	0	0.1	0	0	0
MgO	1.8	0.8	1.7	4.3	2.89	0.1	0	0.2	0.42	0.1
CaO	1.98	2.3	3.5	6.7	4.64	0.7	0.5	0.6	0.46	0.8
Na_2O	4.01	5.2	3.3	3.6	5.11	3.6	3.9	4.9	1.01	4.1
K_2O	2.44	3	1.5	1.4	1.407	3.3	3.6	1.7	6.98	2.5
P_2O_5	0.104	0.1	0.1	0.1	0.12	0.026	0.02	0.1	0.04	0.023
LOI	0.7	0.3	0.5	0.9	0.42	0.3	0.6	0.3	0.43	0.3
Total	100.4	100.5	100.3	100.1	100.9	100.5	100.4	99.7	100.3	100
A/CNK	1.1	0.99	1.01	0.8	0.9	1.09	1.19	1.13	1.51	1.09
Sc	12	16	17	4	23	6	3	9	8	5
V	80	63	99	13	162	18	14	13	10	16
Cr	27	47	43	13	4	10	<1	3.1	59	1.8
Co	11	6	12	<1	23	<0.5	<2	1	3	0.3
Ni	10	0	8	<1	2	<0.5	69	<0.2	5	<1
Cu	7	10	5	<1	26	<2	<4	<3	9	<4
Zn	108	34	25	7	66	14	14	7	70	15
Ga	14	15	15	13	16	12	18	16	10	11
Rb	86	95	54	138	52	71	257	47	125	54
Sr	125	88	145	71	143	121	7	47	63	127
Y	28	24	31	22	26	37	50	52	28	42
Zr	219	142	194	59	110	124	69	98	216	119
Nb	8	4	9	16	3	7	20	12	9	7
Ba	390	345	287	279	159	744	29	473	1952	522
La	22.4	20.7	21	13.5	13.3	43.8	21.8	28.6	68.7	47.6
Ce	46.2	38.2	39	11	27.5	69.3	40.5	63.3	130	74.5
Nd	23.6	17.7	25	4	16.5	26.6	20.8	25.6	44	32.4
Sm	n.d.		5.2	n.d.	n.d.	n.d.	n.d.	n.d.	n.d.	7
Th	9	11	8.3	16	7	15	17.6	21	18	15
Pb	n.d.	12	n.d.	n.d.	n.d.	n.d.	28	7	n.d.	n.d.
U	n.d.	2.2	n.d.	n.d.	n.d.	2	4	3	n.d.	3

Sample no.	Naoussa (NW Paros)				Monasteri (NW Paros)						
	PS-20	PS-27	P-12	P-48b	PS-25	PS-26	PR-3	PR-6	PA-6	PA-7	PA-10
Rock unit	NPG	NPG	NPG	NPG	NPG	NPG	NPG	NPG	NPG	NPG	NPG
(*b*) *Paros basement gneiss*											
SiO_2	70.0	67.29	68.85	71.05	70.013	72.94	71.03	71.907	71.90	73.37	71.03
TiO_2	0.51	0.554	0.42	0.42	0.51	0.25	0.48	0.485	0.48	0.26	0.48
Al_2O_3	14.56	15.93	14.54	14.80	14.86	14.22	14.8	14.64	14.64	14.13	14.89
Fe_2O_3	2.99	4.178	3.52	2.68	3.23	2.05	3.18	3.221	3.22	2.065	3.18
MnO	0.05	0.09	0.08	0.04	0.03	0.04	0.05	0.05	0.05	0.04	0.05
MgO	1.15	1.13	1.31	0.70	1.17	0.45	1.08	1.04	1.04	1.15	1.08
CaO	1.64	1.83	1.98	1.27	1.62	1.44	1.67	1.46	1.46	0.56	1.67

Table 1 continued

Sample no.	Naoussa (NW Paros)				Monasteri (NW Paros)						
	PS-20	PS-27	P-12	P-48b	PS-25	PS-26	PR-3	PR-6	PA-6	PA-7	PA-10
Rock unit	NPG	NPG	NPG	NPG	NPG	NPG	NPG	NPG	NPG	NPG	NPG
Na_2O	3.27	5.40	3.76	3.49	3.93	3.71	3.53	3.36	3.36	2.69	3.53
K_2O	4.62	2.02	3.88	4.88	3.49	3.86	3.17	3.03	3.03	5.46	3.17
P_2O_5	0.22	0.21	0.12	0.19	0.206	0.15	0.19	0.19	0.19	0.07	0.19
LOI	0.65	0.98	0.79	0.81	0.98	0.53	0.79	0.92	0.92	0.71	0.79
Total	99.72	99.65	99.25	100.3	100.07	99.69	100.09	100.33	99.411	100.54	100.09
A/CNK	1.10	1.13	1.05	1.12	1.14	1.12	1.23	1.3	1.3	1.26	1.23
Sc	5	8	13	8	5	5	10	9	9	7	10
V	38	22	54	34	43	19	42	43	43	22	42
Cr	26	7	14	7	15	11	47	10	10	12	47
Co	13	14	9	5	12	8	5	6	6	3	5
Ni	1.2	1	4	2	0.5	1	2	3	3	0.5	2
Cu	n.d	n.d	2.4	5.1	n.d	n.d	0	<1	<1	<1	0
Zn	56	55	54	59	63	49	64	72	72	44	64
Ga	22	17	17	21	22	21	21	20	20	20	21
Rb	180	100	123	160	108	144	94	101	101	196	94
Sr	169	135	107	152	186	142	170	148	148	99	170
Y	18	31	37.3	18.7	22.5	24	20.3	18.8	18.8	14.8	20.3
Zr	249	202	121	175	196	132	184	184	184	141	184
Nb	14	8	10	12	13	13	12	12	12	12	12
Ba	856	313	489	1151	984	606	860	659	659	868	860
La	35.7	14.8	20.2	21.1	28.5	23.6	22.1	25	25	29.8	22.1
Ce	68.7	39.2	41.9	37	66.1	44.2	44.5	47.3	47.3	53	44.5
Nd	50.8	23.8	14.7	14.2	47.3	23.5	34.86	37.7	35.43	32.7	31.1
Sm	9.5	5.2	n.d.	n.d	9.5	6.15	7.11	n.d	7.2	5.5	6.36
Th	17	3	13	13	12	10	9	11	11	17	9
Pb	n.d	n.d	n.d	n.d	n.d	n.d	n.d	n.d	n.d	n.d	n.d
U	n.d	n.d	n.d	n.d	n.d	n.d	n.d	n.d	n.d	n.d	n.d

Sample no.	Monasteri (NW Paros)			Golden beach (E Paros)		Piso Livadhi
	P2	P27a	P16	P33	P34	PA-22
Rock unit	NPG	NPG	NPG	EPG	EPG	EPG
SiO_2	69.61	71.03	72.19	76.38	66.59	n.d
TiO_2	0.50	0.35	0.27	0.12	0.62	n.d
Al_2O_3	14.77	14.58	13.99	13.23	15.19	n.d
Fe_2O_3	3.25	2.47	2.25	0.98	5.11	n.d
MnO	0.05	0.04	0.05	0.02	0.06	n.d
MgO	0.92	0.62	0.76	0.19	1.94	n.d
CaO	1.61	1.54	1.10	0.71	1.48	n.d
Na_2O	5.28	3.95	3.71	4.73	2.25	n.d
K_2O	2.75	3.85	4.58	2.38	3.40	n.d
P_2O_5	0.19	0.18	0.14	0.25	0.22	n.d
LOI	0.53	0.92	0.61	0.98	2.45	n.d
Total	99.46	99.53	99.65	99.97	99.31	n.d
A/CNK	1.03	1.10	1.09	1.17	1.48	n.d

Table 1 continued

Sample no.	Monasteri (NW Paros)			Golden beach (E Paros)		Piso Livadhi
	P2	P27a	P16	P33	P34	PA-22
Rock unit	NPG	NPG	NPG	EPG	EPG	EPG
Sc	9	7	9	5	10	11
V	42	23	19	14	88	40
Cr	22	7	3	19	74	13
Co	6	4	4	1	14	5
Ni	3	1	1	1	33	3
Cu	3	2	2	<1	9	2
Zn	77	42	60	25	83	50
Ga	21	20	21	12	22	18
Rb	81	125	204	72	116	162
Sr	177	180	117	54	102	117
Y	24	23	1	10	30	36
Zr	198	142	140	42	141	170
Nb	12	10	14	5	14	11
Ba	930	705	736	203	641	746
La	27.1	24.2	25.4	6.1	19.4	30.3
Ce	54.2	46.2	54.2	13.7	38	63.8
Nd	17.7	15.7	22.4	3.5	14.1	37.36
Sm	n.d.	n.d.	n.d.	n.d.	n.d.	7.73
Th	10.6	9.2	14	1.2	9	14.9
Pb	n.d	n.d	n.d	n.d	n.d	n.d
U	n.d	n.d	n.d	n.d	n.d	n.d

GQFG grey quartzofeldspathic gneiss, *LG* leucogneiss, *LGr* leucogranite, *NPG* NW Paros gneiss, *EPG* East Paros gneiss. A/CNK as alumina saturation index [$Al_2O_3/CaO + Na_2O + K_2O$] in molar proportions; Sample locations in Fig. 2a, b

In the southernmost peninsula (Cape Spathi, Fig. 2a), there is evidence of a local increase in metamorphic grade up to amphibolite facies, demonstrated by the occurrence of garnet-bearing leucosome layers (Cape Lighthouse, Fig. 2a) which show a granoblastic texture. This is attributed to be the result of in situ partial melting of the host biotite-gneisses (SER 92-28, Table 1).

In order to decipher their petrogenesis, the compositions of the lower-grade mylonitic gneisses of Serifos (upper greenschist facies/lower amphibolite; Iglseder et al. 2009) are plotted on geochemical and isotopic diagrams with the higher (*T*) grade, migmatitic gneiss of NW Paros.

Analytical procedures and results

Fourteen samples of Paros basement gneisses were collected from the NW Paros gneiss area (Monasteri and Naoussa, Fig. 2b; Table 1); two samples were collected from the lower-grade East Paros gneiss unit (Piso Livadi), and one sample from the Central Paros gneiss (purely for oxygen isotope work) (see locations in Fig. 2b); ten samples were also collected from the southernmost part of Serifos island (Fig. 2a; Table 1). All samples were analysed for major- and trace elements using XRF techniques. Of these, 13 samples were further analysed for Sr and Nd isotopes (Table 2). The sampling strategy for the Sr–Nd isotopic analyses aimed at covering the lithological range on both islands, however, focusing in more detail on Paros basement which displays a larger surface outcrop of this unit compared to Serifos. Therefore, it was considered a key area for understanding the architecture of the Cycladic Basement Unit, and a preliminary sampling was performed on Serifos at that stage. Unfortunately, Sr isotopic analyses of Serifos gneiss were successful for only two out the three selected samples. Sample #SER93-50 (grey biotite-gneiss, ascribed to a greywacke protolith) failed to produce Sr isotope ratios.

A selection of 16 samples from both islands was analysed for O isotopes (Table 3).

Samples were jaw crushed and ground to fine powder in an agate mortar prior to analysis. Major elements were determined on fused discs using Rh anode excitation,

Table 2 Sr- and Nd isotopic compositions of bulk gneiss samples from south Serifos and Paros

South Serifos	Lithological Group	$^{87}Rb/^{86}Sr$*	$^{87}Sr/^{86}Sr$(meas.)	$^{87}Sr/^{86}Sr_{(300)}$[1]	Sm	Nd	$^{147}Sm/^{144}Nd$	$^{143}Nd/^{144}Nd_{(m)}$	$^{143}Nd/^{144}Nd_{(300)}$[1]	$\varepsilon_{Nd\ (0)}$	$\varepsilon^{t}\ Nd_{(300)}$
S93-50	GQFG	–	–	–	5.24	25.21	0.1258	0.512126(4)[4]	0.511879	−9.98	−7.29
S93-52[2]	(LG)	1.23	0.716267(6)[3]	0.711009	7.04	35.5	0.1985	0.51220(4)	0.511810	−8.54	−5.62
S93-63	Garnet-Leucogneiss	106.40	0.723957(6)	–	–	20.84	–	0.512198(4)	–	−8.58	–
NW and E Paros gneiss											
PA6	Monasteri (NPG)	1.98	0.717871(6)	0.709380	7.2	35.43	0.1228	0.512122(3)	0.511881	−10.06	−7.25
PA7	Monasteri (NPG)	5.75	0.719462(7)	<0.70	5.55	32.87	0.102	0.512222(4)	0.512022	−8.11	−4.50
PA10	Monasteri (NPG)	1.60	0.716825(7)	0.709978	6.36	31.11	0.1235	0.512132(3)	0.511889	−9.87	−7.08
PS25	Monasteri (NPG)	1.69	0.716686(7)	0.709468	9.47	47.321	0.121	0.512095(4)	0.511857	−10.59	−7.71
PS26	Monasteri (NPG)	2.92	0.723267(6)	0.710779	6.155	n/a	n/a	n/a	n/a	n/a	n/a
PR3	Monasteri (NPG)	1.60	0.716899(7)	0.710052	7.11	34.86	0.1233	0.512129(4)	0.511887	−9.92	−7.13
PR6	Monasteri (NPG)	1.98	0.717837(7)	0.709346	2.99	37.68	0.048	0.512128(4)	0.512034	−9.94	−4.27
PA22	Piso Livadhi (EPG)	4.02	0.722439(6)	0.705274	7.73	37.36	0.1251	0.512207(4)	0.511961	−8.40	−5.68
PS20	Naoussa (NPG)	3.08	0.723871(7)	0.710700	9.495	50.807	0.113	0.512076(4)	0.511854	−10.96	−7.77
PS27	Naoussa (NPG)	2.15	0.715525(7)	0.706322	5.224	23.82	0.1326	0.512370(4)	0.512109	−5.22	−2.79
Average NW Paros gneiss ($n = 9$) 2.52			0.718694	0.709503	5.20	36.73	0.11	0.512159	0.511942	−9.33	−6.06

[1] Initial values calculated at 300 Ma. possible Hercynian age of Serifos orthogneiss (Schneider et al. 2011) and Paros basement gneisses (Engel and Reischmann 1998)

[2] Isotopic data from Stouraiti et al. (2010)

() [3]Value in parenthesis represent the 2σ error on the last digits of the measured $^{87}Sr/^{86}Sr_{(meas.)}$ ratios

() [4]Value in parenthesis represents the 2σ error on the last digits of the measured $^{143}Nd/^{144}Nd_{(meas.)}$ ratios

(meas.) = measured

()* $^{87}Rb/^{86}Sr$ was calculated from Rb/Sr concentrations obtained by XRF based on equation (Faure 1986): $^{87}Rb/^{86}Sr = (Rb/Sr)[2.6939 + 0.2832\ ^{87}Sr/^{86}Sr]$ and using GCDkit software (by Janoušek et al. 2006)

Table 3 Oxygen isotope composition as $\delta^{18}O_{SMOW}$ (‰) of quartz separates from Serifos and Paros mylonitic gneisses

Sample Name	Description	Rock unit	$\delta^{18}O_{SMOW}$ (‰)
South Serifos Gneiss Unit			
S92-28	Biotite Quartz-feldspathic Gneiss (QFG)	Grey Gneiss	12.5(1)
S92-29	Quartz-feldspathic Gneiss	Grey Gneiss	12.7
S93-50	Quartz-feldspathic Gneiss	Grey Gneiss	11.6
S93-52	Leuco-granite	LGr	12.7
SLeuco-2	Leuco-gneiss	LG	12.4
SLeuco-1	Aplite	LG	11.4
S93-61	Mylonitic Orthogneiss	LG	12.2
S93-63	Garnet mylonitic Orthogneiss	LG	11.0
Paros Basement Gneisses and Schists (NW and central Paros)			
PS-20	Gneiss (Naoussa)	NPG	11.9
PS-25	Gneiss (Monasteri)	NPG	11.3
PA-6	Gneiss	NPG	10.4
PA-7	Gneiss	NPG	10.35
PA-10	Gneiss	NPG	10.0
PR-3	Gneiss	NPG	10.8
PR-6	Gneiss	NPG	11.0
PA-72	Mica Schist (Lefkes-central Paros)	CPG	10.4

NPG NW Paros gneiss, *CPG* Central Paros gneiss, *LG* Leucogneiss, *LGr* Leucogranite

(1): Average error of the measurements is ±0.2 ‰

and the trace elements Sc, V, Cr, Ni, Zn, Ga, Rb, Sr, Y, Zr, Nb, La, Ce, Nd, and Ba on pressed powder briquettes using either Rh or W excitation on a Philips PW1600 X-ray fluorescence spectrometer at Leicester University, using the technique of Marsh et al. (1983). Whole-rock analyses for major and trace elements are presented in Table 1.

Sr–Nd isotope ratios were analysed at the NERC Isotope Geosciences Laboratory (NIGL, Keyworth). Sr and Nd were separated from common dissolutions of 150-400 mg powdered samples using ultra-clean reagents and conventional cation exchange columns. Procedural blanks for Sr, Nd, and Sm averaged ca. 500 pg, ca. 126 pg and ca. 341 pg, respectively, during the period of analysis.

Sr isotopic compositions were measured in static mode on a Finnigan MAT 262 mass spectrometer (TIMS instrument), whilst Nd isotopic composition was measured both in static mode on the Finnigan and in dynamic mode on a VG 354 mass spectrometer (TIMS instrument). $^{87}Sr/^{86}Sr$ was normalized to $^{86}Sr/^{88}Sr = 0.1194$, and $^{143}Nd/^{144}Nd$ was normalized to $^{146}Nd/^{144}Nd = 0.7219$. Within-run precision for Sr and Nd isotope ratios, expressed as one standard error of the mean, was 0.000007 and 0.000005 for $^{87}Sr/^{86}Sr$ and $^{143}Nd/^{144}Nd$, respectively.

Results for isotope standards during the period of these measurements were: NBS 987 $^{87}Sr/^{86}Sr = 0.710195 \pm 0.000011$ ($n = 10$), Seawater $^{87}Sr/^{86}Sr = 0.709117 \pm 0.000007$ ($n = 12$), Johnson-Matthey Nd $^{143}Nd/^{144}Nd = 0.511127 \pm 0.000007$ ($n = 15$) and La Jolla Nd $^{143}Nd/^{144}Nd = 0.511851 \pm 0.000008$ on the VG 354 ($n = 10$) and 0.511871 ± 0.000007 ($n = 9$) on the Finnigan (all errors: one standard deviation). Internal errors on individual measurements were always much smaller than the standard reproducibility reported here, and therefore, the ability to reproduce the standards should be taken as the limiting factor in interpreting the uncertainty of any given analysis.

Oxygen isotope ratios of quartz separates were determined at the NERC Isotope Geoscience Laboratory, on aliquots of ~5 mg, employing the oxygen liberation technique of Clayton and Mayeda (1963), using ClF_3 instead of BrF_5 (Borthwick and Harmon 1982). The oxygen yields were converted to CO_2 by reaction with a heated graphite rod. CO_2 isotope ratios were measured on a CJS Science Ltd Phoenix 390 mass spectrometer. Measurements are reported as δ notation per mil (‰), representing deviations relative to the SMOW (Standard Mean Ocean Water) standard for $^{18}O/^{16}O$. The $\delta^{18}O_{SMOW}$ results were normalized with the NIGL laboratory standard and quoted relative to NBS#28 (African sand) at a value of 9.63 ‰. Currently, determined values for NBS#28 are x ± 1σ. Standard reproducibility was estimated at just over ±0.2 ‰. The average error of the unknown is ±0.2 ‰ and for the standard ±0.17 ‰.

Bulk-rock geochemistry

The major- and trace-element analyses for Serifos and Paros gneisses are listed in Table 1. In this section, major oxide data are compared with respect to the chemical

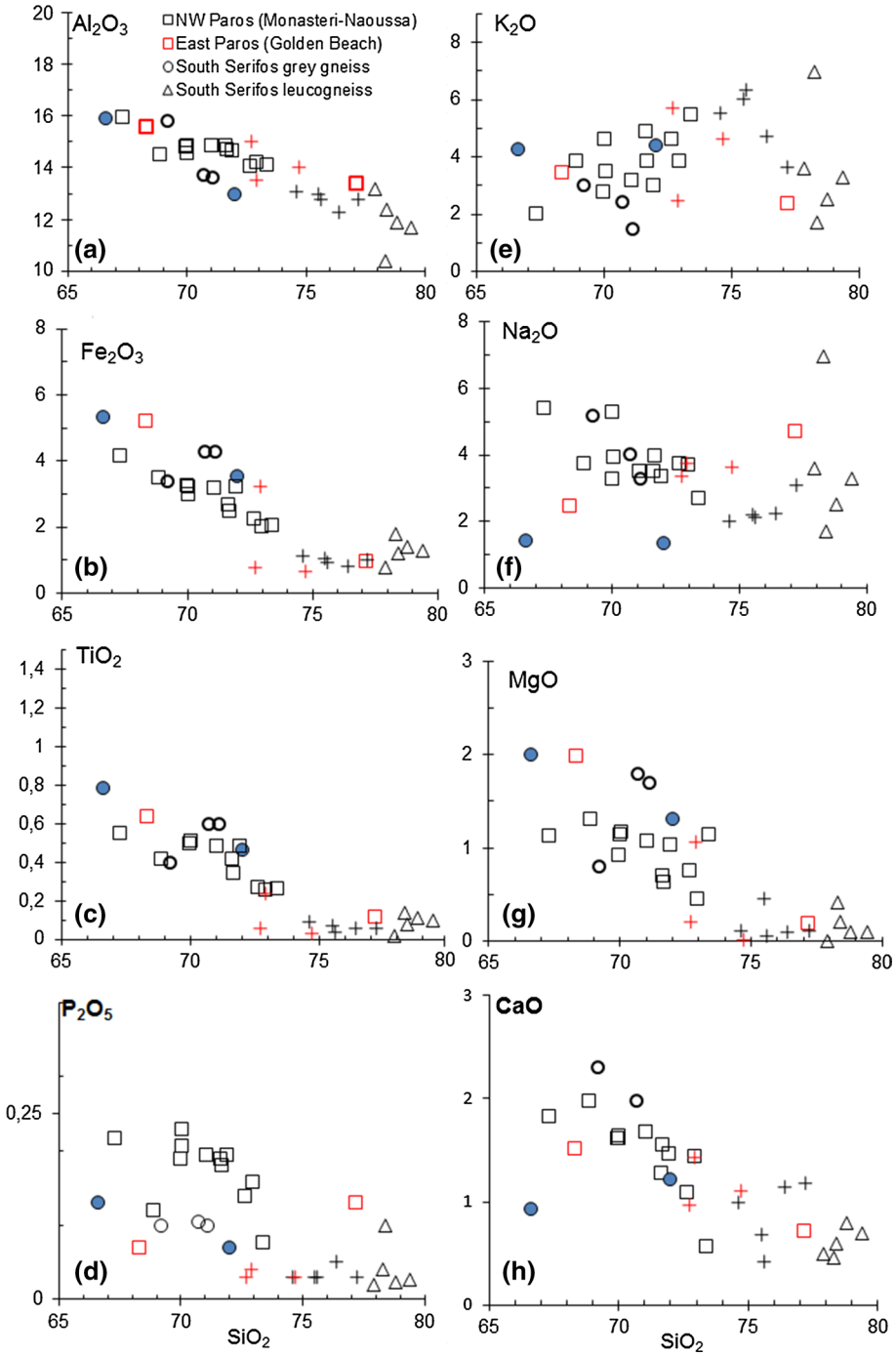

Fig. 3 **a–h** Harker diagrams for major elements versus SiO_2 displaying compositional variations of mylonitic gneisses from the Serifos and Paros basement units. For comparisons, data are provided from Naxos paragneiss (*blue circles*), migmatite (*red crosses*) and the leucogranite core (*black crosses*). Data from Pe-Piper et al. (1997)

characterization of the potential sedimentary and igneous protoliths of the Serifos and Paros Cycladic Basement gneisses.

Paros Cycladic Basement gneiss

NW Paros gneiss from Monasteri and Naoussa display limited variation in SiO_2 (67.3–73.3 wt%) and Al_2O_3 (13.2–16 wt%, Fig. 3), whilst all NW Paros gneiss samples are mildly to highly peraluminous (A/CNK = 1.05–1.3; Fig. 4; Table 1). This high peraluminosity is consistent with the presence of minor amounts of aluminosilicate minerals including cordierite and sillimanite. One mica schist sample from the East Paros gneiss area (#P34, Table 1), which is considered to be derived from a pelite-rich metasedimentary protolith, has the highest A/CNK value (1.48, Fig. 4) and displays strong similarities to paragneisses from the Naxos Lower Unit (data from Pe-Piper et al. 1997).

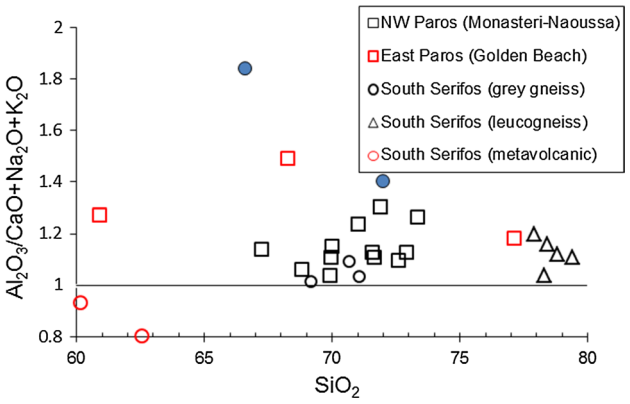

Fig. 4 Silica (wt%) versus $Al_2O_3/CaO + Na_2O + K_2O$ (A/CNK) in molar proportions as an aluminosity index for Paros and Serifos basement gneisses. Naxos Hercynian paragneisses (metapelites in blue circles are plotted for comparison (Pe-Piper et al. 1997). Dashed-line is boundary of S-type/I-type granite from Chappell and White (1992), and solid line is the peraluminous-metaluminous boundary of Shand (1927)

Most major oxides and trace elements, e.g. TiO_2, Al_2O_3, Fe_2O_3(t), MgO (Fig. 3) and Cr, Ni, Sc, V, Rb, Ba, Ta, Zr, Nb, Th show negative correlation with SiO_2. The decrease in Fe_2O_3(t), MgO, TiO_2, and Sc (elements that are indicative of ferromagnesian minerals) in the gneisses is not coupled with an obvious increase in CaO–Na_2O–Sr (elements that are indicative of feldspars). Commonly siliciclastic sedimentary sequences display a decrease in the ferromagnesian mineral/feldspars ratio with increasing SiO_2 (Shaw 1956; Taylor and McLennan 1985; Sawyer 1986), but this is not observed in the NW Paros sequence.

The South Serifos grey gneiss

The grey gneisses are felsic rocks that span the fields of granite and granodiorite on the normative Ab–An–Or plot (Fig. 5b). They show a metaluminous affinity (A/CNK: from 1 to 1.08 < 1.1; Fig. 4), high Na_2O (>3.2%), $Na_2O > K_2O$ and low P_2O_5 content (~0.1 wt%, Table 1; Fig. 3). These observations are at variance with an S-type granite signature and more resemble an I-type granitoid (according to the typology of Chappell and White 1974; White and Chappell 1977). Two samples of the South Serifos grey gneiss (S93-53 and S92-26, Table 1) are biotite-rich rocks that are the most mafic rocks of this group with a minor occurrence within this unit. The latter rocks show an intermediate composition (60–62% SiO_2), with a metaluminous (A/CNK range from 0.8 to 0.9; Fig. 4) affinity and magnesian composition (FeOt/FeOt + MgO: 0.47–0.7). In thin-section, these samples display a homogeneous and fine-grained fabric, with a mineral assemblage and chemical characteristics that indicate a sub-volcanic protolith, of intermediate composition (dacite).

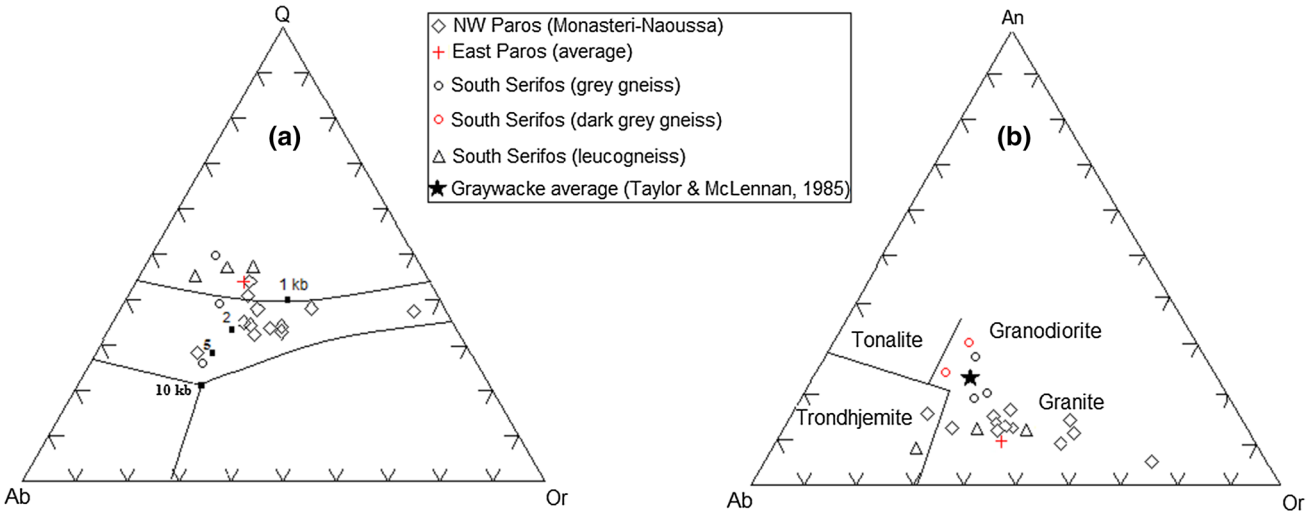

Fig. 5 **a** Geochemical classification of analysed Paros and Serifos gneisses with normative Quartz (Qz)—Albite (Ab)—Orthoclase (Or) contents. Minimum (*dots*) and eutectic melt compositions (*solid lines*) at water-saturated conditions and pressures 1, 2, 5, 10 kb in the system Qz–Ab–Or are from Ebadi and Johannes (1991). Note that the majority of NW Paros gneiss compositions plot close to the minimum melt at 2 kb and point towards undersaturated compositions (orthoclase end), whilst their quartz contents remain the same. **b** Normative albite (Ab)—anorthite (An)—orthoclase (Or) contents of Serifos and Paros gneisses. The Ab–An–Or classification for silicic rocks is after Barker (1979; *bold lines*). One sample of Serifos leucogneiss (SLeu-2) and one from Naoussa (PS27) plot within the trondhjemite field and resemble granitic melts that were generated at water-fluxed conditions at 6 Kbar (Patiño Douce and Harris 1998). The Serifos grey quartzo-feldspathic gneisses span the field of granodiorite, whereas Paros samples span the field of granite. For comparison, the composition of average greywacke (after Taylor and McLennan 1985) is also shown. Note that only the Serifos grey gneiss samples plot close to the average greywacke

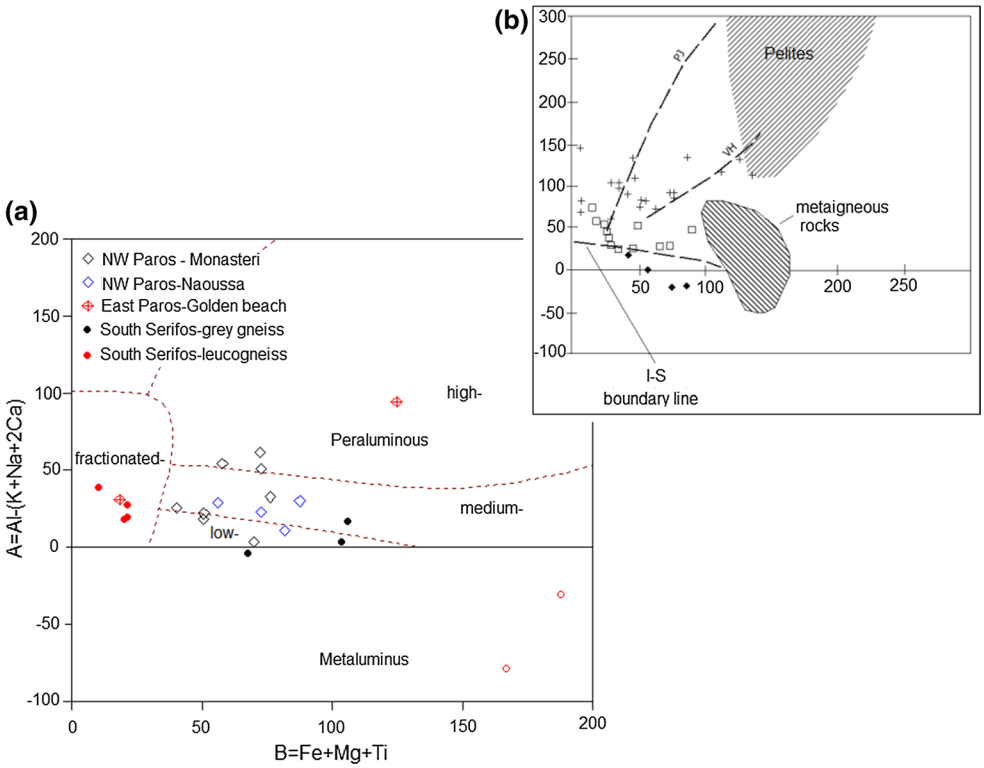

Fig. 6 **A–B** diagram of Debon and Le Fort (1983) modified by Villaseca et al. (1998) for Serifos and Paros gneisses (*open red circles* correspond to the South Serifos basement metavolcanic rocks). I–S *boundary line* is drawn from I-S-types from the Lachlan Fold Belt (Chappell and White 1992). The *inset* shows the fields and trends of experimental granitic melts produced from pelitic and metaigneous protoliths (by Villaseca et al. 1998, and references therein)

The South Serifos leucogneiss

These rocks display a granitic composition as shown in the normative albite–anorthite–orthoclase plot of Fig. 5b. One sample (leucosome, S Leu-2, Table 1) plots towards the Na-enriched Ab corner of Fig. 5b, within the trondjhemite field. We interpret this Na-enrichment to result from alteration (albitization) of plagioclase, and not to represent a primary igneous feature. The South Serifos leucogneiss samples are highly fractionated rocks, with SiO_2 contents (Fig. 3) from 78 to 79.4 wt% and a peraluminous (A/CNK > 1.1, Fig. 4) composition. Their major element variations define the high SiO_2 end of a common trend with other anatectic granites and migmatites from the Lower Unit of the Naxos migmatite gneiss dome (Figs. 3, 4).

The major-element composition of Serifos grey gneiss and leucogneiss may therefore reflect either a) the composition of the original protolith, or b) a protolith that has undergone element mobilization before or during metamorphism (the M1 and M2 events) (Fig. 6).

Trace elements

Several authors have considered that trace elements from the High-Field-Strength (HFSE) group (Zr, Hf, Nb, Ta, Ti, P) (Saunders et al. 1980) and especially the transition metals (Cr, Ni, Sc, V) are relatively immobile during secondary alteration of igneous rocks (Jenner 1996; Hinchey and Carr 2007). Therefore, these elements are more likely to reflect the primary protolith composition and are now further examined in order to deduce the nature of the Serifos and Paros gneiss units.

On mantle-normalized diagrams (Fig. 7a–c), all gneiss units (Serifos and Paros) exhibit enrichments in K, Rb, Ba, (U and Pb) relative to HFSE (e.g. Zr, Nb, Ti and P) and negative anomalies in Ba, Sr, P, and Ti. Ultimately, these patterns resemble the average upper continental crust (Fig. 7a–c).

In order to examine the variations between the different gneiss groups from Paros and Serifos, their bulk compositions were normalized to average UCC (Rudnick and Gao 2003). Figure 8a–d show these data compared with published data for known gneiss groups from the Naxos gneiss dome (Fig. 8f) and also a non-metamorphosed greywacke sequence (Fig. 8e) from the northern Aegean (Chios Lower Unit: Meinhold et al. 2007).

Paros Cycladic Basement gneisses

Northwest Paros and east Paros gneiss showed a significant consistency in trace-element spidergram patterns, with significant enrichment in large highly charged cations which implies contributions from granite-gneisses, sedimentary, and metasedimentary rocks, typical for the upper crust (Fig. 8a, b).

In detail, the NW Paros gneiss samples are enriched in K and Rb, Ba, and Th (about 1–2.5 times the UCC, Fig. 8a)

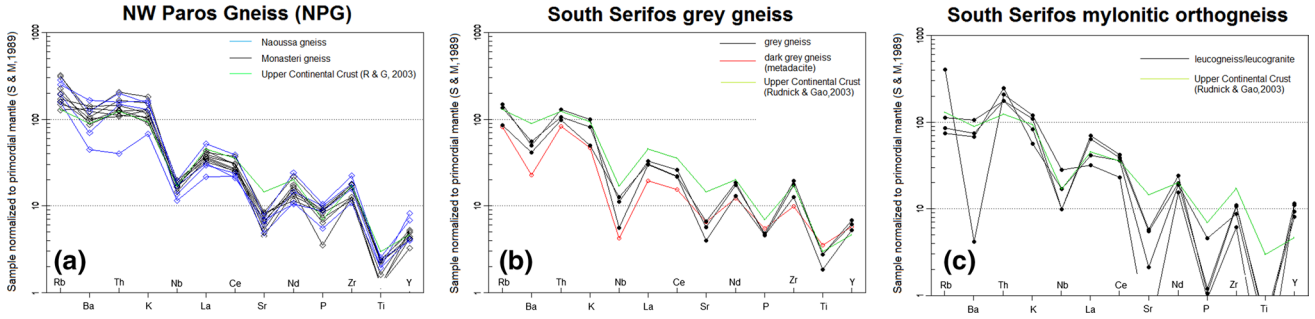

Fig. 7 Primordial mantle-normalized multi-element diagrams (spidergrams) for **a** NW Paros (NPG). *Blue lines* correspond to Naoussa samples; **b** Serifos GQFG and **c** Leucogneiss (LG). *Green line* represents the normalized composition of Upper Continental Crust of Rudnick and Gao (2003). Primordial mantle normalization values by Sun and McDonough (1989)

and depleted with respect to Sr, Ca and Cr, V, Sc, Ti. The loss of Ca, Sr (and Na) alongside the addition of K, Rb, and Ba is typical for highly weathered and recycled (clastic) residues and have been attributed to fixation of the large cations (Rb, Cs, Ba, and K) by ion exchange and adsorption and may therefore reflect the recycled metasedimentary nature of the protolith (Nesbitt et al. 1980). The NW Paros gneiss samples also exhibit low concentrations of Cr (7–46 ppm) and Ni (1–3 ppm), with Cr/Ni ratios >3. The low abundance of the immobile transition metals (Ti, Sc, V, Cr and Ni) in conjunction with the low Cr/V (<1) and high Cr/Ni ratios (>3) is therefore interpreted as a characteristic of a ferromagnesian-poor metasedimentary source rock (Garver et al. 1996). Spidergram patterns of the East Paros gneiss samples (e.g. P34, Fig. 8b) and the Naxos paragneisses (metapelites) share the same Large Ion Lithophile Element (LILE) enrichments and Sr–Ca depletions as the NW Paros gneiss samples (Fig. 8b) which supports their potential common origin. However, in contrast to the NW Paros gneiss, the mica-rich intervals of the East Paros gneiss (interpreted to be derived from a shale-rich, pelitic protolith) have distinctly higher Cr (74–86 ppm) and Ni (34–43 ppm) (Samples P34 and P36, Table 1). The Cr–Ni signature of the East Paros gneiss is highly suggestive of a larger input of mafic volcanic detritus. This rock type (#P34, Golden Beach, Fig. 8b) shows a similar chemical composition to greywacke rocks (Fig. 8b, e).

South Serifos Cycladic Basement gneiss

In general, the South Serifos grey gneiss (Fig. 8c) displays a flat slope with minor variations in elemental patterns when normalized to UCC, alongside lower concentrations of the LILE relative to the NW and East Paros gneisses and Naxos granitic gneiss (Fig. 8e). These rocks well match the geochemical pattern of Chios greywackes (Fig. 8e) and have almost the same concentrations as estimated by Rudnick and Gao (2003) for the upper continental crust (UCC). Calcium and strontium are only slightly depleted compared with UCC. Their metaluminous and magnesian characteristics, alongside their high CaO and Na_2O contents and similarity to rocks produced experimentally from melts of meta-igneous composition (see section "Bulk rock geochemistry"; Fig. 6; Villaseca et al. 1998), are consistent with derivation from an I-type granitoid protolith, with calc-alkaline affinities.

The South Serifos leucogneiss group (Fig. 8d) and granitic gneisses from the core of the Naxos dome (Fig. 8e) display similar, highly fractionated geochemical patterns relative to the UCC, e.g. the largest negative anomalies for Ba, Sr, P, and Ti, and thus, they define a distinct geochemical group. This group exhibits variable enrichments in the radioactive elements K, Th, and U, characteristic negative anomalies for Sr and Ba, and lower concentrations of Zr, Ti and the light rare earth elements (LREE) La and Ce, Nd, relative to average UCC values. This is a characteristic pattern of fractionated granitic gneisses and is typically observed in peraluminous S-type leucogranites (Villaseca et al. 2007; Villaros et al. 2009). Refractory accessory minerals such as monazite or allanite (which sequester the LREE and Y) and zircon (which sequester Zr and Th) do not participate in melting reactions, and thus, most of the REE and HFSE budget is retained within the source rock rather than supplied to the melt fraction (Bea 1996a, b; Ayres and Harris 1997). The larger Ba depletion in the Naxos leucogranites (Fig. 8e) indicates late-stage K-feldspar fractional crystallization from a granitic melt. Interestingly, Serifos leucogneisses do not display K–Ba fractionations except for one sample (S Leu-2, Fig. 8d), indicating incomplete separation of partial melts (leucosomes); field evidence also supports this observation.

Whole-rock Sr and Nd isotope geochemistry

Rubidium–strontium and Sm–Nd data for whole-rock samples from the NW and East Paros gneiss as well as a few

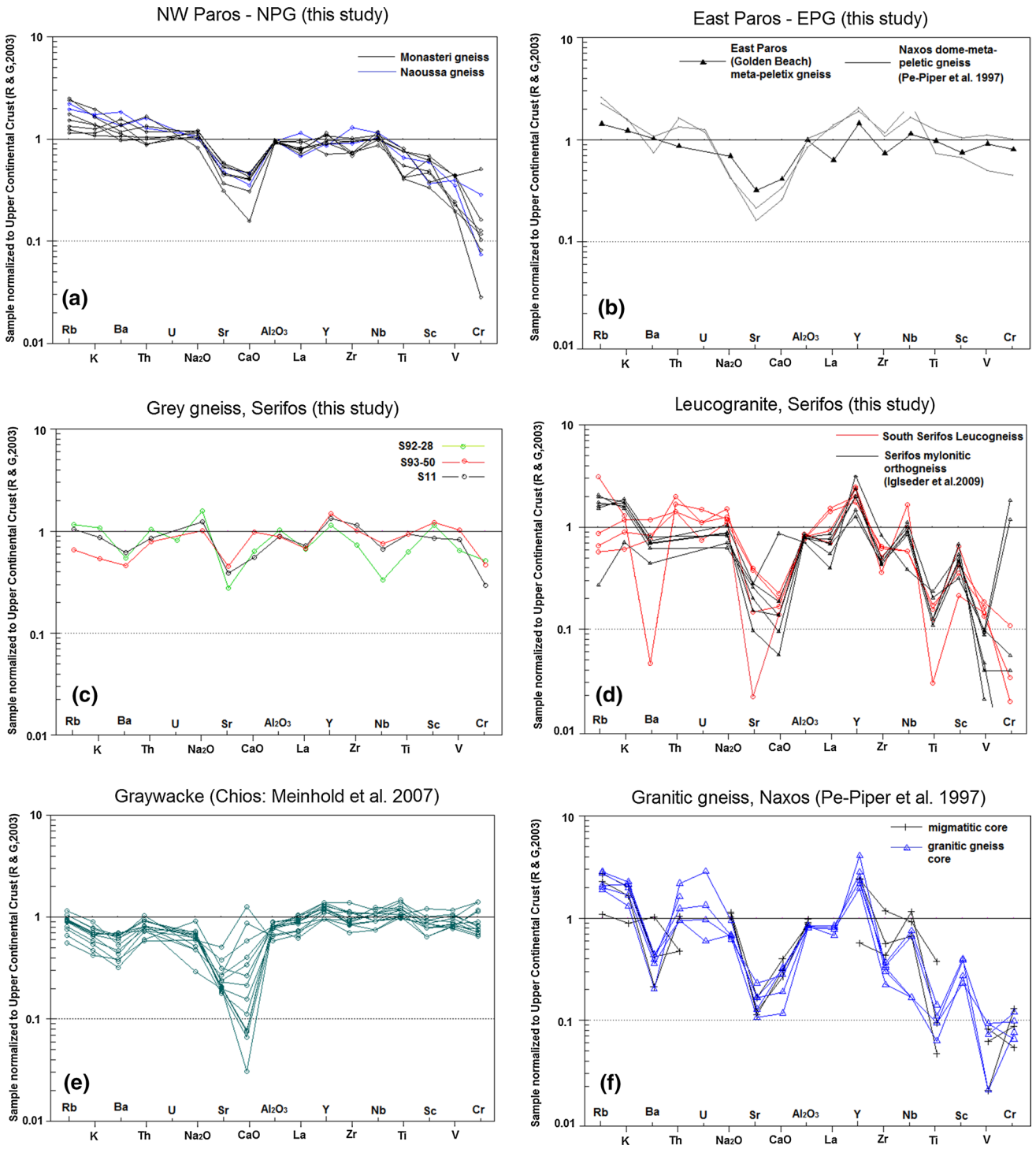

Fig. 8 Spidergrams for Paros, Naxos and Serifos Cycladic Basement gneisses normalized to the average composition of upper continental crust (UCC) after Rudnick and Gao (2003). **a** Monasteri and Naoussa (*blue line*)—NPG; **b** East Paros gneiss (EPG) from Golden Beach compared with metapelites from the Naxos gneissic core (Pe-Piper et al. 1997); **c** South Serifos grey quartzofeldspathic gneiss (GQFG); **d** Leucogneisses and leucogranites from South Serifos and mylonitic orthogneisses from Iglseder et al. (2009) are plotted for comparison; **e** Greywackes of Permo-Triassic age from Chios Lower Unit, N Aegean (data from Meinhold et al. 2007); **f** Granitic gneiss core and migmatitic core from the Naxos gneiss dome (data from Pe-Piper et al. 1997)

samples from southern Serifos are presented in Table 2; Figs. 9, 10. The literature data for the Serifos leucogneiss (Iglseder et al. 2009) are plotted (Fig. 9a) for comparison. Initial Sr and Nd isotopic ratios were calculated for a 300 Ma age, which approximates the age for the Hercynian granitic precursors of the Cycladic Basement orthogneisses (Engel and Reischmann 1998; Schneider et al. 2011). Calculated initial ε_{Nd} values for the Paros–Serifos gneiss at the approximate age of the igneous precursor (t = 300 Ma) vary between −2.8 and −7.8 (Table 2), implying contributions from dominantly felsic crustal sources.

Moreover, for most samples of Paros gneiss (NW and East Paros gneiss) and South Serifos gneisses (one sample of grey gneiss and two samples of leucogneiss), the $(^{87}Sr/^{86}Sr)_i$ values are 0.706–0.711. In general, $\varepsilon_{Nd}(t)$ of the studied samples is low and the lowest $\varepsilon_{Nd}(t)$ values are displayed by the South Serifos leucogneiss and grey gneiss (−7.2 to −8.6). Such values clearly indicate significant contributions of supra-crustal components or an S-type granitoid (S-Supracrustal, according to the typology of Chappell and White 1992). The highest $\varepsilon_{Nd}(t)$ value of −2.7 is from an equigranular gneiss from NW Paros (sample PS27, Table 2) which provides evidence for another potential source, possibly an I-type (igneous) granitoid protolith.

Two leucogneiss samples from the South Serifos show unrealistically low $(^{87}Sr/^{86}Sr)_i$ values (<0.70) due to the very low Sr concentration and high Rb/Sr ratio of these samples (see section "Re-setting of the Rb–Sr system in the Serifos mylonitic orthogneiss").

O isotopes

O isotopic compositions were measured on quartz separates from seven samples of the NW Paros gneiss, one sample of the central Paros gneiss and eight samples from Serifos (Fig. 2a; Table 3). The Paros samples were selected in order to examine isotopic changes within and at various distances from the centre of the main Paros gneiss dome (Fig. 2b; Table 3). $\delta^{18}O_{SMOW}$ (quartz separates) values for Serifos samples show a small range from +11 to +12.7 ‰; samples from Paros display a similar range, varying from +10 to +11.9 ‰. These values are comparable to quartz values from equivalent high-grade gneisses (amphibolite facies) and granites from the Lower Unit core of the Naxos migmatitic gneiss dome (values ca. +10.6 to 11.8 ‰; Baker and Matthews 1995; Figs. 2c, 10). High O isotope ratios of this type are a common characteristic of the Hercynian granites of Western Europe (Sheppard 1977; Wickham 1990).

Oxygen isotope data from Paros basement gneiss do not indicate a spatial gradation of oxygen isotopes in relation to the dome geometry (i.e. with increased distance from the core of the Central Paros gneiss dome). The data rather

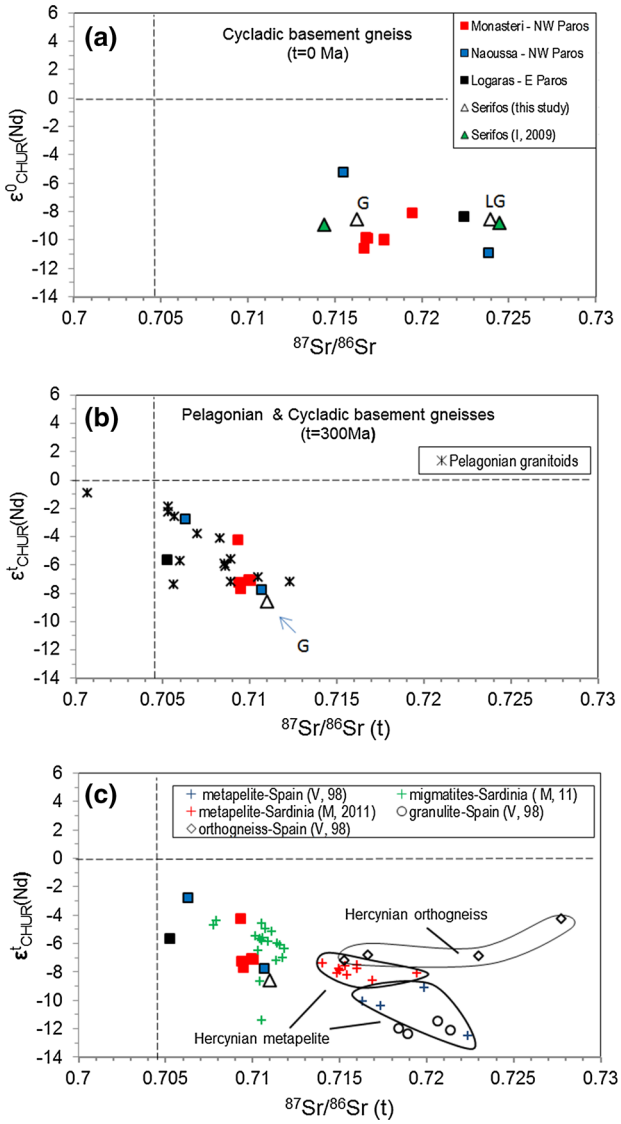

Fig. 9 **a** Present day $^{87}Sr/^{86}Sr$ versus ε_{Nd} of Paros and Serifos gneisses. Note that most Monasteri samples plot at the high radiogenic Sr—end of the variation in quadrant IV. **b** Initial $^{87}Sr/^{86}Sr$ versus initial ε_{Nd} (calculated at 300 Ma) correlation diagram for Cycladic samples (Serifos and Paros from this study) and Pelagonian basement granitoids (data from Anders 2005). **c** Hercynian belt gneisses from central Spain (Villaseca et al. 1998) and Sardinia (Macera et al. 2011) plot alongside migmatites and anatexites derived from other Hercynian Sardinian metasedimentary sources (All data are age-corrected at 300 Ma)

reflect the pre-metamorphic isotopic variation of the variable metasedimentary (inter-bedded psammitic and pelitic layers) and metaigneous protoliths. Homogenization and lowering of $\delta^{18}O_{SMOW}$ values in the Monasteri gneiss unit of the NW Paros gneiss can be attributed to intense mylonitization during the M1/D1 and M2/D2 events. In Fig. 10, $\delta^{18}O_{SMOW}$ values of the NW Paros gneiss are similar to those of the Naxos Lower Unit migmatitic core.

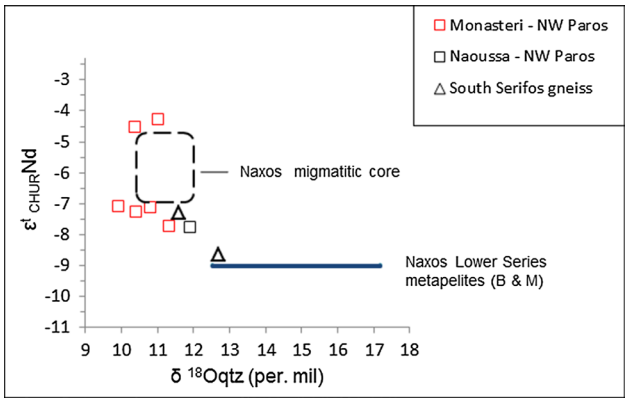

Fig. 10 Correlation of initial ε_{Nd} versus $\delta^{18}O_{SMOW}$ (‰) for Paros and Serifos Cycladic Basement gneisses (from this study). The *schematic box* illustrates the range in ε_{Nd}–$\delta^{18}O_{SMOW}$ values (quartz separates and quartz veins) of the leucogneiss core of the Naxos dome (O isotope values of Lower Series rocks from Naxos metamorphic basement from Baker and Matthews 1995; Nd isotope data from Pe-Piper 2000)

Discussion

Nature of the crustal protoliths of mylonitic gneisses and provenance

A comparison of major and trace-element characteristics of the Cycladic basement quartzofelspathic gneisses and metasediments of the present study with those of well-defined Hercynian age granitoids and Mesozoic sedimentary suites might help to constrain the provenance of the Cycladic metamorphic rocks.

The observed negative trends of Fe_2O_3(t), MgO, TiO_2 and Sc (Fig. 3) with increasing silica content and the lack of an obvious increase in CaO–Na_2O–Sr argue against a siliciclastic sedimentary protolith (Sawyer 1986; Taylor and McLennan 1985) for the NW Paros gneiss (Fig. 3). Nevertheless, chemical differentiation during migmatitization of quartzofeldspathic and pelitic rocks, and especially dehydration reactions at upper amphibolites facies conditions, would consume ferromagnesian minerals (e.g. biotite) and plagioclase to produce melt and K-feldspar ± garnet (Le Breton and Thompson 1988). This process would result in a decrease in Fe_2O_3(t), MgO, TiO_2, CaO and an increase in K_2O, with increasing silica content, as observed in the NW Paros gneiss (Fig. 3). This argument is further supported by the overlapping fields and a broad common evolutionary trend of the NW Paros gneiss with the paragneisses and migmatites from the Lower Unit core of the Naxos dome (Fig. 2c; Pe-Piper et al. 1997; Pe-Piper 2000), with increasing silica content (Fig. 3).

Migmatization and local anatexis are manifest in the NW Paros gneiss by the formation of common tourmaline-bearing pegmatite veins. In addition, most NW Paros gneisses have the appropriate composition for producing granitic melts, as bulk-rock compositions plot close to the minimum melt composition, at 2–5 kb and water-undersaturated conditions, in the haplogranite system Q–Ab–Or (Ebadi and Johannes 1991; Fig. 5a).

The South Serifos grey gneiss display an unusually large variation of K_2O (1.4–6.98 wt%) and Na_2O (1–5.1 wt%), with highly variable K_2O/Na_2O ratios and low P_2O_5 contents. Such geochemical features are interpreted to reflect metasomatic processes in these mylonitic rocks. Similar metasomatic trends in Na, K, and P have been reported for Triassic mylonitic granitic gneisses within the Cycladic Blueschist Unit of southern Evia, Attic-Cycladic Massif (Chatzaras et al. 2013). The composition of the South Serifos grey gneiss is similar to that of rocks produced experimentally from melts of meta-igneous rather than pelitic protoliths (Fig. 6 and inset diagram, Villaseca et al. 1998). However, a greywacke protolith cannot be ruled out and is further examined below.

Discrimination factors based on major- and trace-element data were identified for different tectonic settings of Palaeozoic greywackes from eastern Australia (Bhatia 1983; Bhatia and Crook 1986). These settings which can be identified on the basis of the geochemical signature of sedimentary-rock suites include data of oceanic island arc (OIA), continental island arcs (CIA), active continental margins (ACM), and passive margins (PM). Also, Permo-Triassic greywackes from Chios (northern Aegean) are used (data from Meinhold et al. 2007) as a reference for the composition of clastic sedimentary sequences from the Aegean region. In the double-ternary plot (Th–Sc–Zr/10 and Th–La–Sc) (Fig. 11), Serifos grey gneiss exclusively plot in the field of CIA, as well as the majority of NW Paros gneiss. A minor group of NW Paros and Serifos leucogneiss-granite plot in the field of ACM, whereas one pelite-rich sample from E Paros and a metavolcanite from S Serifos fall in the field of OIA. The data support a dominant felsic source for the NW Paros gneiss and Serifos leucogneiss and a more mafic source (OIA) for the pelite-rich units of E Paros.

Regional geochemical correlations

A significant feature of Sr–Nd systematics seen in Fig. 9b, c is the steeply sloping trend displayed by the NW and East Paros gneiss and South Serifos leucogneiss. This pattern differs from the flat trends observed in other Hercynian basement rocks, e.g. Spanish and Sardinian Hercynian

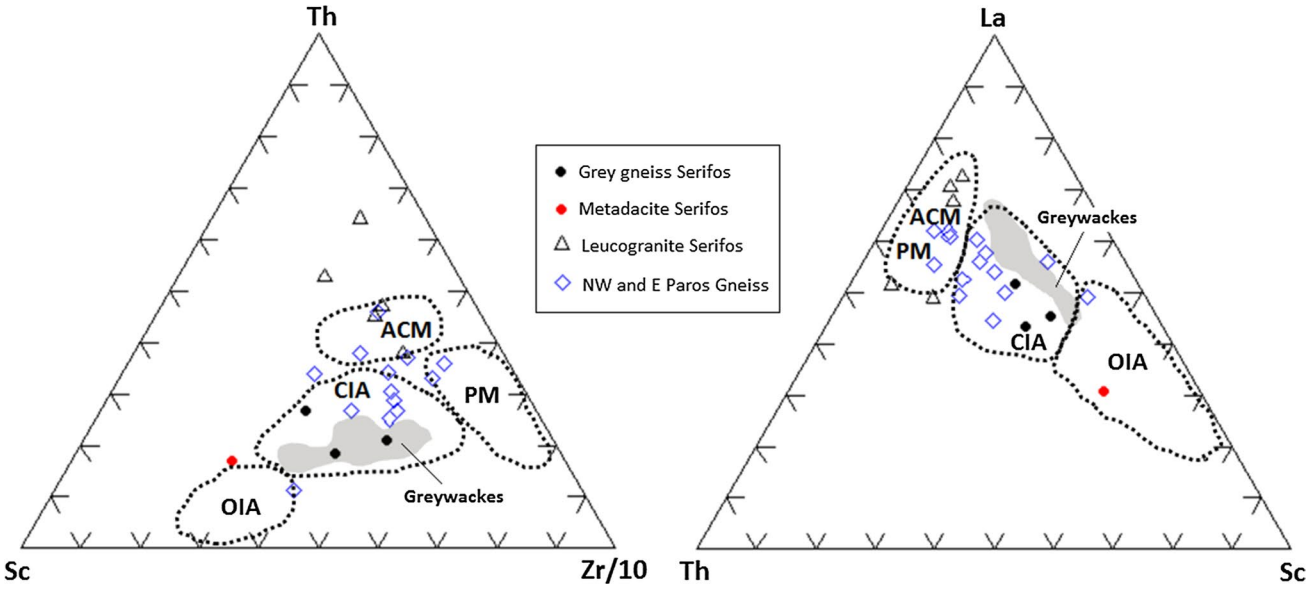

Fig. 11 Ternary diagrams La–Th–Sc and Th–Sc–Zr = 10 with discrimination fields of tectonic setting, after Bhatia and Crook (1986). Light-grey field represent data of Permo-Triassic greywackes of Chios N. Aegean (data from Meinhold et al. 2007). *OIA* Oceanic island arc, *CIA* continental island arc, *ACM* active continental margin, *PM* passive margins

metapelites and Spanish orthogneiss (Fig. 9c; Villaseca et al. 1998), but it closely resembles that of migmatites and anatexites from other Hercynian metasedimentary terranes, e.g. Sardinia (Fig. 9c) (Macera et al. 2011). Moreover, evidence from U to Pb geochronology of detrital and inherited zircons from metasedimentary, gneissic and meta-igneous basement rocks of the Cyclades (Keay and Lister 2002) showed that the Cycladic age pattern is similar to the European Variscides.

Compared with other pre-Alpine basement rocks from continental Greece, the Sr–Nd isotopic variation of Paros and Serifos basement rocks overlap with Hercynian basement meta-granitoids from the Pelagonian zone (Anders 2005) in northern Greece (Fig. 9b). Both Cycladic and Pelagonian granitoids exhibit a common trend towards less radiogenic Sr and higher initial ε_{Nd} isotopic ratios, indicating a mixed crustal source made up of mafic (juvenile)-to-felsic (supracrustal) rocks in different proportions.

According to previous studies, most Carboniferous granitoids in the Aegean have similar geochemical characteristics in accordance with a volcanic arc setting in an active continental margin (Vavassis et al. 2000; Pe-Piper and Piper 2002; Peytcheva et al. 2004; Xypolias et al. 2006; Tomaschek et al. 2008). They are peraluminous granodiorites and granites that display similarities to I- and S-type granites, indicating that plutonism took place within a subduction zone setting (e.g. Peytcheva et al. 2004). These similarities have been interpreted to indicate that during the Late Carboniferous, the pre-Alpine basement of the Cyclades was in close proximity to the Pelagonian and External Hellenides (e.g., Kithira, SW Aegean).

Available data for acid-intermediate meta-igneous rocks from a variety of orogenic belts exhibit a lowering in Sr–Nd compositions towards bulk earth values, when compared to the same metamorphic rocks in upper crustal levels, e.g. central Spain (Villaseca et al. 1998) and the French Massif Central (Downes and Duthou 1988). Bickle et al. (1988) showed that Sr isotopic ratios are profoundly affected by high-grade metamorphism and anatexis, as in the case of Paros and Naxos gneiss domes. In this case, metapelites and orthogneisses may preserve major and trace-element compositions, but the Sr isotopic ratios may be significantly modified, depending on whether they equilibrate at lower or upper crustal levels.

Despite the paucity of systematic Sr–Nd–O isotopic data available for the Cycladic basement gneisses, comparisons of isotopic data from this study, together with data from the Naxos gneiss dome, have yielded consistent and systematic similarities in their chemistry. The clear similarities in trace-element patterns and ε_{Nd} (300)–δO_{qtz} (Fig. 10) isotope characteristics between the high-grade peraluminous gneisses from NW and East Paros and paragneisses from the Lower Unit of the Naxos dome (Pe-Piper 2000) corroborate a common origin for the metasedimentary units that form the metamorphic core complexes in central Cyclades.

Re-setting of the Rb–Sr system in the Serifos mylonitic orthogneiss

Calculations of initial Sr isotope values for the most fractionated leucogranitic gneisses (>75% SiO_2) of South Serifos (this study) and two mylonitic orthogneiss from Iglseder et al. (2009) failed to produce meaningful values (<0.700), except for one leucogranite sample (#S93-52) from a layered gneiss (Initial Sr = 0.713, see Table 2). Younger ages (200 or 150 Ma) were tested in calculations, but did not produce realistic initial Sr ratios for the South Serifos leucogneisses.

The unrealistically low initial Sr isotopic ratios in fractionated granitoids, as displayed by the Serifos mylonitic orthogneiss, are usually ascribed to post-magmatic isotopic alteration and disturbance of the Rb–Sr system (Moreno-Ventas et al. 1995). An explanation for such a low $(^{87}Sr/^{86}Sr)_i$ (<0.7) is a secondary increase in the Rb/Sr ratio as a result of Sr loss during metamorphism, as suggested by the very low Sr concentration of some of the South Serifos leucogneiss samples (e.g. Sr = 7 ppm for sample S93-63, Table 1), which could be attributed to feldspar alteration. Recrystallization of the matrix minerals of the Serifos gneisses during mylonitization may have resulted in re-setting of the whole-rock Rb–Sr system. Such re-setting phenomena in the Rb–Sr isotope systems are known from fault zones within orogenic belts, where zones of mylonitization and cataclasis are formed (Fullagar 1992), as is observed in the southern and central part of the Serifos core complex (Grasemann and Petrakakis 2007; Rabillard et al. 2015).

Conclusions

1. Mylonitic rocks of the Cycladic Basement Unit gneiss from NW and Eastern Paros and from Serifos (the southern Serifos grey gneiss) contain various lithological groups within their protoliths. The gneissose basement rocks from both islands have similar textural attributes, but despite this, they have quite different protoliths. Identification of protoliths is extremely difficult in most areas of southern Serifos due to pervasive overprinting during the Eocene (M1/D1) compressional event and the subsequent M2/D2 extensional tectono-thermal episode and metasomatism. Some degree of characterization of the pre-metamorphic precursors is feasible by combining mineralogy, bulk-rock chemistry, and in particular, the immobile trace elements, with Sr–Nd–O isotopes and making comparisons with lower-grade rocks from the Cycladic basement from Paros and Naxos.
2. Coherent trends defined by major elements versus SiO_2 in the NW Paros gneiss group indicate a progression in the degree of migmatization of the original East Paros gneiss (lower grade) metasedimentary (greywacke/semi-pelitic) protolith, towards the (higher grade) more felsic and homogenized composition of the NW Paros (Monasteri) gneiss.
3. Trace-element patterns, alongside the mineral assemblage and small grain size (due to mylonitization) of the South Serifos grey gneiss, reveal that these rocks cannot be equivocally ascribed to a single protolith, either granitoid or greywacke. However, the metaluminous and calc-alkaline affinity and spidergram patterns displayed by this group is rather consistent with a greywacke protolith and derivation from an arc-type felsic igneous rock.
4. Mylonitic leucogneiss-granite layers are common in southern Serifos, having a distinct trace-element pattern characterized by highly fractionated LILE relative to the HFS elements, similar to S-type granites and migmatites from the nearby metamorphic core complex of Naxos.
5. Combined high $\delta^{18}O$ values (+10 to +12.9 ‰), initial $^{87}Sr/^{86}Sr$ (0.706–0.710) and negative ε_{Nd} (t) (<−4.2) values for the NW Paros gneiss, and South Serifos grey gneiss indicate that their source rocks were largely recycled sedimentary and metasedimentary rocks. Sr–Nd isotopic variations across Paros gneiss dome enable us to identify a broad increase in initial Nd isotope ratios and decrease in Sr isotopes values—as the grade of metamorphism increases—towards the centre of the gneiss domes of Paros. This trend is clearly shown by the NW Paros gneisses of Monasteri and Naoussa. Sr–Nd systematics of the NW Paros (Naoussa) gneisses indicate contributions from a different source, either of lower crustal origin or mixing of the upper crustal component with a mantle-derived magmatic component.

Acknowledgements We would like to thank professor John Tarney (University of Leicester) for his assistance, guidance, and support of this study. Field and analytical work were supported by the State Scholarship Foundation of Greece, ΙΔΡΥΜΑ ΚΡΑΤΙΚΩΝ ΥΠΟΤΡΟΦΙΩΝ (IKY), and the isotope analyses by the Natural Environment Research Council (NERC; UK). The valuable assistance of Nick Marsh at the University of Leicester (XRF analysis) is greatly appreciated. The authors thank professors Hilary Downes and Michael Bröcker for their constructive comments that helped improve this manuscript. We also appreciate the very helpful suggestions and comments by the Editor-in-Chief professor Wolf-Christian Dullo and the topic-Editor professor Ingo Braun for editorial handling. Furthermore, we thank Dr. Kostantinos Soukis for useful comments and Dr. Danae Antivachis for helping with figures.

References

Altherr R, Kreuzer H, Wendt I, Lenz H, Wagner GA, Keller J, Harre W, Höhndorf A (1982) A late oligocene/early miocene high temperature belt in the attic-cycladic crystalline complex (SE Pelagonian, Greece). Geol Jahrb 23:97–164

Anders B (2005) The pre-Alpine evolution of the basement Zone and the Vardar Zone, Greece. Unpublished Ph.D. thesis, Johannes-Gutenberg-Universität Mainz, Germany

Anders B, Reischmann T, Kostopoulos D (2007) Zircon geochronology of basement rocks from the Pelagonian Zone, Greece: constraints on the pre-Alpine evolution of the westernmost Internal Hellenides. Int J Earth Sci 96:639–661

Andriessen PAM, Boelrijk NAIM, Hebeda EH, Priem ENA, Verdurmen EATh, Verschure RH (1979) Dating the events of metamorphism and granitic magmatism in the Alpine orogen of Naxos (Cyclades, Greece). Contrib Mineral Petrol 69:215–225

Andriessen PAM, Banga G, Hebeda EH (1987) Isotopic age study of pre-alpine rocks in the basal units on Naxos, Sikinos and Ios, Greek Cyclades. Geol Mijnbouw 66:3–14

Ayres M, Harris N (1997) REE fractionation and Nd-isotope disequilibrium during crustal anatexis: constraints from Himalayan leucogranites. Chem Geol 139:249–269

Baker J, Matthews A (1995) The stable isotopic evolution of a metamorphic complex, Naxos, Greece. Contrib Mineral Petrol 120:391–403

Bargnesi EA, Stockli DF, Mancktelow N, Soukis K (2013) Miocene core complex development and coeval supradetachment basin evolution of Paros, Greece, insights from (U–Th)/He thermochronometry. Tectonophysics 595–596:165–182

Barker F (1979) Trondhjemites, dacites, and related rocks. Elsevier, Amsterdam

Bea F (1996a) Controls on the trace element composition of crustal melts. Geol Soc Am Spec Pap 315:33–41

Bea F (1996b) Residence of REE, Y, Th and U in granites and crustal protoliths: implications for the chemistry of crustal melts. J Petrol 37:521–552

Bhatia MR (1983) Plate tectonics and geochemical compositionof sandstones. J Geol 91:611–627

Bhatia MR, Crook KAW (1986) Trace element characteristics of graywackes and tectonic setting discrimination of sedimentary basins. Contrib Mineral Petrol 92:181–193

Bickle MJ, Wickham SM, Chapman HJ, Taylor HP Jr (1988) A strontium, neodymium and oxygen isotope study of hydrothermal metamorphism and crustal anatexis in the Trois Seigneurs Massif, Pyrenees, France. Contrib Mineral Petrol 100:399–417

Bolhar R, Ring U, Allen CM (2010) An integrated zircon geochronological and geochemical investigation into the Miocene plutonic evolution of the Cyclades, Aegean Sea, Greece: part 1: geochronology. Contrib Mineral Petrol 160:719–742. doi:10.1007/s00410-010-0504-4

Borthwick J, Harmon RS (1982) A note regarding ClF3 as alternative to Br F5 for oxygen isotope analysis. Geochim Cosmochim Acta 46:1665–1668

Brichau S, Thomson S, Ring W (2010) Thermochronometric constraints on the tectonic evolution of the Serifos detachment, Aegean Sea. Int J Earth Sci 99:379–393. doi:10.1007/s00531-008-0386-0

Bröcker M, Franz L (1998) Rb–Sr isotope studies on Tinos Island (Cyclades, Greece): additional time constraints for metamorphism, extent of infiltration-controlled overprinting and deformational activity. Geol Mag 135:369–382

Bröcker M, Keasling A (2006) Ion probe U–Pb zircon ages from the high-pressure/low-temperature melange of Syros, Greece: age diversity and the importance of pre-Eocene subduction. J Metamorph Geol 24:615–631

Bröcker M, Pidgeon RT (2007) Protolith ages of meta-igneous and metatuffaceous rocks from the Cycladic Blueschist Unit, Greece: results of a reconnaissance U–Pb zircon study. J Geol 115:83–98

Bröcker M, Huyskens M, Berndt J (2016) U–Pb dating of detrital zircons from Andros, Greece: constraints for the time of sediment accumulation in the northern part of the cycladic blueschist belt. Geol J 51:354–367

Buick IS (1991) The late Alpine evolution of an extensional shear zone, Naxos, Greece. J Geol Soc Lond 148:93–103

Buick IS, Holland TJB (1989) The P-T-t path associated with crustal extension, Naxos, Cyclades, Greece. Geological Society, London, Special Publications 43:365–369

Chappell BW, White AJR (1974) Two contrasting granite types. Pac Geol 8:173–174

Chappell BW, White AJR (1992) I- and S-type granites in the Lachlan fold belt. Trans R Soc Edinb Earth Sci 83:1–26

Chatzaras V, Dörr W, Finger F, Xypolias P, Zulauf G (2013) U–Pb single zircon ages and geochemistry of metagranitoid rocks in the Cycladic Blueschists (Evia Island): implications for the Triassic tectonic setting of Greece. Tectonophysics 595–596:125–139

Clayton RN, Mayeda TK (1963) The use of bromine pentafluoride in the extraction of oxygen from oxides and silicates for isotopic analysis. Geochim Cosmochim Acta 27:43–52

Debon F, Le Fort P (1983) A chemical-mineralogical classification of common plutonic rocks and associations. Trans R Soc Edinb Earth 73:135–149

Downes H, Duthou JL (1988) Isotopic and trace element arguments for the lower-crustal origin of Hercynian granitoids and pre-Hercynian orthogneisses, Massif Central (France). Chem Geol 68:291–308

Dürr S, Altherr R, Keller J, Okrusch M, Seidel E (1978) The median Aegean crystalline belt: stratigraphy, structure, metamorphism, magmatism. In: Closs H et al (eds) Alps, apennines, hellinides, inter-union commission on geodynamics scientific report 38, E. Schweizerbart'sche Verlagsbuchhandlung, Stuttgart, pp 455–477

Ebadi A, Johannes W (1991) Beginning of melting and composition of first melts in the system Qz–Ab–Or–H_2O–CO_2. Contrib Mineral Petrol 106:286–295

Engel M, Reischmann T (1998) Single zircon geochronology of orthogneisses from Paros, Greece. Bull Geol Soc Greece 32:91–99

Faure G (1986) Principles of Isotope Geology. Wiley, New York, p 589

Franz L, Okrusch M, Bröcker M (1993) Polymetamorphic evolution of pre-Alpidic basement rocks on the island of Sikinos (Cyclades, Greece). Neues Jahrb Mineral Monatshefte 4:145–162

Fu B, Bröcker M, Ireland T (2015) Zircon U–Pb, O, and Hf isotopic constraints on Mesozoic magmatism in the Cyclades, Aegean Sea, Greece. Int J Earth Sci 104:75–87. doi:10.1007/s00531-014-1064-z

Fullagar PD (1992) Geochronological studies of fault-related rocks. In: Bartholomew MJ, Hyndman DH, Mogk DW, Mason R (eds) Basement Tectonics, 8, Characterization and Comparison of Ancient and Mesozoic Continental Margins, Proceedings of the Eighth International Conference on Basement Tectonics, Montana, USA, 1988, pp 37–50

Garver JI, Royce PR, Smick TA (1996) Chromium and nickel in shale of the Taconic foreland: a case study for the provenance of fine-grained sediments with an ultramafic source. J Sediment Res 66:100–106

Gautier P, Brun JP (1994) Crustal-scale geometry and kinematics of late-orogenic extension in the central Aegean (Cyclades and Ewia Island). Tectonophysics 238:399–424

Gautier P, Brun JP, Jolivet L (1993) Structure and kinematics of Upper Cenozoic extensional detachment on Naxos and Paros (Cyclades Islands, Greece). Tectonics 12:1180–1194

Grasemann B, Petrakakis K (2007) Evolution of the Serifos metamorphic core complex. In: Lister G, Forster M, Ring U (eds) Inside

the Aegean metamorphic core complexes. J Virtual Explor, 28, Paper 2
Grasemann B, Schneider DA, Stockli DF, Iglseder C (2011) Miocene bivergent crustal extension in the Aegean: evidence from the western Cyclades (Greece). Lithosphere 4:23–39
Henjes-Kunst F, Kreuzer H (1982) Isotopic dating of pre-alpidic rocks from the island of Ios (Cyclades, Greece). Contrib Mineral Petrol 80:245–253
Hinchey AM, Carr SD (2007) Protolith composition of cordierite–gedrite basement rocks and garnet amphibolites of the Bearpaw Lake area of the Thor–Odin Dome, Monash Complex, British Columbia, Canada. Can Mineral 45:607–629
Hinsken T, Bröcket M, Berndt J, Gärtner C (2015) Maximum sedimentation ages and provenance of metasedimentary rocks from Tinos Island, Cycladic blueschist belt, Greece. Int J Earth Sci. doi:10.1007/s00531-015-1258-z
Iglseder C, Grasemann B, Schneider DA, Petrakakis K, Miller C, Klötzli US, Thöni M, Zámolyi A, Rambousek C (2009) I and S-type plutonism on Serifos (W-Cyclades, Greece). Tectonophysics 473:69–83
Janoušek V, Farrow CM, Erban V (2006) Interpretation of whole-rock geochemical data in igneous geochemistry: introducing Geochemical Data Toolkit (GCDkit). J Petrol 47(6):1255–1259
Jenner GA (1996) Trace-element geochemistry of igneous rocks; geochemical nomenclature and analytical geochemistry. In: Wyman DA (ed) Trace-element geochemistry of volcanic rocks: applications for massive sulphide exploration. Geological Association of Canada, Short Course Notes 12:51–77
Jolivet L, Brun JP (2010) Cenozoic geodynamic evolution of the Aegean. Int J Earth Sci 99:109–138
Jolivet L, Faccenna C, Goffé B, Burov E, Agard P (2003) Subduction tectonics and exhumation of high-pressure metamorphic rocks in the Mediterranean orogens. Am J Sci 303:353–409
Jolivet L, Menant A, Sternai P, Rabillard A, Arbaret L, Augier R, Laurent V, Beaudoin A, Grasemann B, Huet B, Labrousse L, Le Pourhiet L (2015) The geological signature of the slab tear below the Aegean. Tectonophysics 659:166–182
Katzir Y, Garfunkel Z, Avigad D, Matthews A (2007) The geodynamic evolution of the Alpine orogen in the Cyclades (Aegean Sea, Greece): insights from diverse origins and modes of emplacement of ultramafic rocks. Geol Soc Lond Spec Publ 291:17–40
Keay S, Lister G (2002) African provenance for the metasediments and metaigneous rocks of the Cyclades, Aegean Sea, Greece. Geology 30:235–238
Keay S, Lister G, Buick I (2001) The timing of partial melting, Barrovian metamorphism and granite intrusion in the Naxos metamorphic core complex, Cyclades, Aegean Sea, Greece. Tectonophysics 342:275–312
Le Breton N, Thompson AB (1988) Fluid-absent (dehydration) melting of biotite in metapelite in the early stages of crustal anatexis. Contrib Mineral Petr 99:226–237
Lister GS, Banga G, Feenstra A (1984) Metamorphic core complexes of Cordilleran type in the Cyclades, Aegean Sea, Greece. Geology 12:221–225
Löwen K, Bröcker M, Berndt J (2015) Depositional ages of clastic metasediments from Samos and Syros, Greece: results of a detrital zircon study. Int J Earth Sci 104:205–220
Macera P, Di Pisa A, Gasperini D (2011) Geochemical and Sr-Nd isotope disequilibria during multi-stage anatexis in a metasedimentary Hercynian crust. Eur J Mineral 23:207–222
Marsh NG, Tarney J, Hendry GL (1983) Trace element geochemistry of basalts from hole 504B, Panama Basin, DSDP Legs 69 and 70. Initial Rep Deep Sea 69:747–763
Martin L, Duchêne S, Deloule E, Vanderhaeghe O (2006) The isotopic composition of zircon and garnet: a record of the metamorphic history of Naxos, Greece. Lithos 87:174–192
McGrath A (1999) Structural and geochemical evolution of an extensional metamorphic core complex, Paros, Greece. Unpubl Ph.D. thesis. University of Leicester, UK
Meinhold G, Kostopoulos D, Reischmann T (2007) Geochemical constraints on the provenance and depositional setting of sedimentary rocks from the islands of Chios, Inousses and Psara, Aegean Sea, Greece: implications for the evolution of Palaeotethys. J Geol Soc Lond 164:1145–1163
Moreno-Ventas I, Rogers G, Castro A (1995) The role of hybridization in the genesis of Hercynian granitoids in the Gredos Massif, Spain: inferences from Sr–Nd isotopes. Contrib Mineral Petrol 120:137–149
Nesbitt HW, Markovics G, Price RC (1980) Chemical processes affecting alkalis and alkaline earth during continental weathering. Geochim Cosmochim Acta 44:1659–1666
Okrusch M, Bröcker M (1990) Eclogite facies rocks in the Cycladic Blueschist Belt, Greece: a review. Eur J Mineral 2:451–478
Papanikolaou DJ (1977) On the structural geology and tectonics of Paros Island (Aegean Sea). Ann Geol de Pays Hell 28:450–464
Papanikolaou DJ (1980) Contribution to the geology of the Aegean Sea: the island of Paros. Ann Geol de Pays Hell 30:65–96
Papanikolaou D (1987) Tectonic evolution of the Cycladic blueschist belt (Aegean Sea, Greece). Chem Transp Metasomatic Process. Springer, Netherlands, pp 429–450
Papanikolaou D (1989) Are the medial crystalline massifs of the Eastern Mediterranean drifted Gondwanan fragments? Geol Soc Greece Spec Publ 1:63–90
Papanikolaou DJ, Demirtasli E (1987) Geological correlations between the Alpine segments of the Hellenides–Balkanides and Taurides–Pontides. In: Flugel HW et al (eds) Pre-variscan and Variscan events in the Alpine-Mediterranean mountain belts. Allfa Publishers, Bratislava, pp 387–396
Patiño Douce AE, Harris N (1998) Experimental constraints on Himalayan anataxis. J Petrol 39:689–710
Pe-Piper G (1998) The nature of Triassic extension-related magmatism in Greece: evidence from Nd and Pb isotope geochemistry. Geol Mag 135:331–348
Pe-Piper G (2000) Origin of S-type granites coeval with I-type granites in the Hellenic subduction system, Miocene of Naxos, Greece. Eur J Mineral 12:859–875
Pe-Piper G, Piper DJW (2002) The igneous rocks of Greece: the anatomy of an orogen. Gebrüder Borntraeger, Berlin
Pe-Piper G, Kotopouli CN, Piper DJW (1997) Granitoid rocks of Naxos, Greece: regional geology and petrology. Geol Mag 32:153–171
Petrakakis K, Iglseder C, Zámolyi A, Rambousek C, Grasemann B, Draganits E, Kurka A, Photiades A (2010) Geological map of Greece, Serifos Island. Institute of Geology and Mineral Exploration, Athens
Peytcheva I, von Quadt A, Ovtcharova M (2004) Metagranitoids from the eastern part of the Central Rhodopean Dome (Bulgaria): U–Pb, Rb–Sr, and Ar–Ar timing of emplacement and exhumation and isotope-geochemical features. Contrib Mineral Petrol 82:1–31
Photiades A, Keay A (2003) Geological and geochronological data for Sikinos and Folegandros metamorphic units (Cyclades, Greece): their tectono-stratigraphic significance. Bull Geol Soc Greece 35:35–45
Rabillard A, Arbaret L, Jolivet L, Le Breton N, Gumiaux C, Augier R, Grasemann B (2015) Interactions between plutonism and detachments during metamorphic core complex formation, Serifos Island (Cyclades, Greece). Tectonics 34:1080–1106. doi:10.1002/2014TC003650
Reischmann T (1998) Pre-alpine origin of tectonic units from the metamorphic core complex of Naxos, Greece, identified by single zircon Pb/Pb dating. Bull Geol Soc Greece 32:101–111

Robertson AHF (2012) Late Palaeozoic–Cenozoic tectonic development of Greece and Albania in the context of alternative reconstructions of Tethys in the Eastern Mediterranean region. Int Geol Rev 54:373–454

Rudnick RL, Gao S (2003) Composition of the continental crust. In: Holland HD, Turekian KK (eds) Treatise on geochemistry, vol 3. Elsevier-Pergamon, Oxford, pp 1–65

Saunders AD, Tarney J, Marsh NG, Wood DA (1980) Ophiolites as ocean crust or marginal basin crust: a geochemical approach. In: Panayiotou A (ed) Ophiolites. Proceedings of the international ophiolite symposium, cyprus 1979, pp 193–204

Sawyer EW (1986) The influence of rock type, chemistry, chemical weathering and sorting on the geochemistry of clastic sediments from Quetico Metasedimentary Belt, Superior Province, Canada. Chem Geol 55:77–95

Schneider DA, Senkowski C, Vogel H, Grasemann B, Iglseder C, Schmitt AK (2011) Eocene tectonometamorphism on Serifos (western Cyclades) deduced from zircon depth-profiling geochronology and mica thermochronology. Lithos 125:151–172

Shand SJ (1927) Eruptive rocks. Murby, London

Shaw DM (1956) Geochemistry of pelitic rocks. Part II: major elements and general geochemistry. Geol Soc Am Bull 67:919–934

Sheppard SMF (1977) The Cornubian batholiths, southwest England: D/H and $^{18}O/^{16}O$ studies of kaolinite and other alteration minerals. J Geol Soc Lond 133:573–591

Stouraiti C, Mitropoulos P, Tarney J, Barreiro B, McGrath AM, Baltatzis E (2010) Geochemistry and petrogenesis of late Miocene granitoids, Cyclades, southern Aegean: nature of source components. Lithos 114:337–352

Sun S-S, McDonough WF (1989) Chemical and isotopic systematics of oceanic basalts: implications for mantle composition and processes, Geological Society, London, Special Publications 42:313–345

Taylor SR, McLennan SM (1985) The continental crust: its composition and evolution. Blackwell, Oxford

Tomaschek F, Keiter M, Kennedy AK, Ballhaus C (2008) Pre-alpine basement within the Northern Cycladic Blueschist unit on Syros Island, Greece. Z dtsch Ges Geowiss 159:521–532

Tschegg C, Grasemann B (2009) Deformation and alteration of a granodiorite during low-angle normal faulting (Serifos, Greece). Lithosphere 1:139–154

Van der Maar PA, Jansen JBH (1983) The geology of the polymetamorphic complex of Ios, Cyclades, Greece, and its significance for the Cycladic Massif. Geol Rundsch 72:283–299

Van Hinsbergen DJJ, Hafkenscheid E, Spakman W, Meulenkamp JE, Wortel R (2005) Nappe stacking resulting from subduction of oceanic and continental lithosphere below Greece. Geology 33:325–328

Vavassis I, De Bono A, Stampfli GM, Giorgis D, Valloton A, Amelin Y (2000) U–Pb and Ar–Ar geochronological data from the Pelagonian basement in Evia (Greece): geodynamic implication for the evolution of Paleotethys. Schweiz Miner Petrogr 80:21–43

Villaros A, Stevens G, Moyen JF, Buick IS (2009) The trace element compositions of S-type granites: evidence for disequilibrium melting and accessory phase entrainment in the source. Contrib Mineral Petrol 158:543–561

Villaseca C, Barbero L, Rogers G (1998) Crustal origin of Hercynian peraluminous granitic batholiths of Central Spain: petrological, geochemical and isotopic (Sr, Nd) constraints. Lithos 43:55–79

Villaseca C, Orejana D, Paterson BA, Billstrom K, Pérez-Soba C (2007) Metaluminous pyroxene-bearing granulite xenoliths from the lower continental crust in central Spain: their role in the genesis of Hercynian I-type granites. Eur J Mineral 19:463–477

White AJR, Chappell BW (1977) Ultrametamorphism and granitoid genesis. Tectonophysics 43:7–22

Wickham SM (1990) Isotopic modification of the continental crust: implications for the use of isotope tracers in granite petrogenesis. In: Asworth JR, Brown M (eds) High-temperature Metamorphism and Crustal Anatexis. Unwin Hyman, London, pp 124–148

Wijbrans JR, McDougall I (1988) Metamorphic evolution of the Attic Cycladic metamorphic belt on Naxos (Cyclades, Greece) utilizing 40Ar/39Ar age spectrum measurements. J Metamorph Geol 6:571–594. doi:10.1111/j.1525-1314.1988.tb00441.x

Xypolias P, Dörr W, Zulauf G (2006) Late carboniferous plutonism within the pre-Alpine basement of the external hellenides (Kithira, Greece): evidence from U–Pb zircon dating. J Geol Soc Lond 163:539–547